Archives of Civil and Mechanical Engineering (2023) 23:154
https://doi.org/10.1007/s43452-023-00688-6

REVIEW ARTICLE

A review on numerical modelling techniques in friction stir processing: current and future perspective

Roshan Vijay Marode[1] · Srinivasa Rao Pedapati[1] · Tamiru Alemu Lemma[1] · Mokhtar Awang[1,2]

Received: 8 November 2022 / Revised: 27 April 2023 / Accepted: 1 May 2023 / Published online: 28 May 2023

Abstract

Friction stir processing (FSP) has gained significant attention worldwide since its inception due to its remarkable solid-state characteristics and microstructure refinement. However, the complex geometry of the FSP and 3-D features makes it challenging to create a set of governing equations for analyzing the post-process theoretical behavior. Due to significant deformation, experiments cannot provide comprehensive information throughout the real process, which frequently entails expense, resources, and time; numerical analysis has been examined extensively over the former to solve these concerns. Numerous alternative processes are to be simulated using FSP's numerical analysis before physical testing to better understand the impact of various system characteristics. An attempt has been made to explore the latest research on the development of various numerical modelling techniques that lead to meaningful insight to enhance the performance of FSP. An advanced numerical technique for studying the influence of different field variables, changes in tool orientation on material flow coupled with appropriate surface contact involving temperature-dependent coefficient of friction values using advanced smoothed particle hydrodynamics on a GPU hardware configuration is still in future scope. This necessity to develop thermo-mechanical models of surface composites facilitates accurate prediction of the thermal record and particle dispersion in FSP. This article compiles computational approaches, the potential of different FEA software, and other post-processing parameters, viz., heat generation, temperature distribution, and material transition. In this regard, some vital challenges and issues regarding the numerical approaches of friction stir processing remain to be addressed, and opportunities for future research prospects are thus recommended.

Keywords Friction stir processing · Numerical analysis · Computational approaches · Thermo-mechanical behavior · Modelling techniques

List of symbols

MMC's	Metal matrix composites
AS	Advancing side
RS	Retreating side
TRS	Tool rotational speed
TTS	Tool traverse speed
Q	Heat generation
SPH	Smoothed particle hydrodynamics
σ	Material flow stress
A	Quasi-static yield strength
B	Strain hardening constant
C	Strengthening coefficient
m	Thermal softening coefficient
n	Strain hardening coefficient
ε	Equivalent plastic strain
$\dot{\varepsilon}$	Plastic strain rate
$\dot{\varepsilon}_o$	Reference plastic strain rate
T_{room}	Ambient temperature
T_{melt}	Melting temperature
PD	Plunge depth
TTA	Tool tilt angle
T_p	Peak temperature
B_4C	Boron carbide
SiC	Silicon carbide
ZrO_2	Zirconium oxide/zirconia
Gr	Graphite
MWCNTs	Multi-walled carbon nanotubes
TiC	Titanium carbide

✉ Srinivasa Rao Pedapati
psrao@ymail.com

[1] Department of Mechanical Engineering, Universiti Teknologi PETRONAS, 32610 Seri Iskandar, Perak, Malaysia

[2] Institute of Transport Infrastructure, Universiti Teknologi PETRONAS, 32610 Seri Iskandar, Perak, Malaysia

FVM	Finite volume method
CEL	Coupled-Eulerian–Lagrangian
HAZ	Heat-affected zone
SZ	Stir zone
TMAZ	Thermo-mechanically affected zone
BM	Base material
FDM	Finite difference method

1 Introduction

Automobile, aerospace, and marine are the key sectors in the transportation industries that demand lightweight design structures. The necessity for tailored material qualities and lightweight characteristics is propelling the development of manufacturing processes. Friction stir technology is an essential element of the engineering processes for manufacturing lightweight components. In 1991, The Welding Institute pioneered Friction Stir Welding (FSW) [1], a simple and efficient process for joining metals and alloys. FSW results in a strong joint with excellent material properties, which is difficult to achieve in traditional welding techniques. FSP is the modified version of FSW, conceived by Mishra et al. [2] in 1999. FSP functions on the same mechanical principle as FSW, like the identical setup, a non-depleting tool equipped with a shoulder and pin. The tool provides a revolving movement with a descending force, and the tool pin lowers into the material until the shoulder strikes the top layer to be processed. Immense heat is produced at the top layer of a workpiece and surrounding material as the tool–workpiece, where friction [3] aids in the plastic deformation and becomes adaptable for producing surface composites [4]. The tool is subsequently given the traverse speed, which helps process the workpiece in a specific direction. The nature of the technique is thermomechanical and helps substantially refine the base material's grain size [5]. It involves modifying the texture and microstructure of the metal through dynamic recovery, discontinuous dynamic recrystallization, and homogeneous mixing at a semi-solid state. Therefore, manufacturing defects attributed to melting, like thermal cracks, voids, blowholes, porosity, loss of strength, etc., are reduced.

Soon after the invention of FSW/FSP technology, many applications were developed and demonstrated successfully in aircraft, defense, and automobile structures [6] for multifunctional products by reinforcing particles [7], compatible with other conventional processes to produce nanostructured materials [8], with ultrasonic vibrations for improving material flow [9], in producing functionally graded materials [10]. Figure 1 depicts the fundamental premise of FSP. The moving pin locally deforms heated material, whereas the rotating shoulder generates most heat via friction with the workpiece. The chamber at the back of the tool is filled with

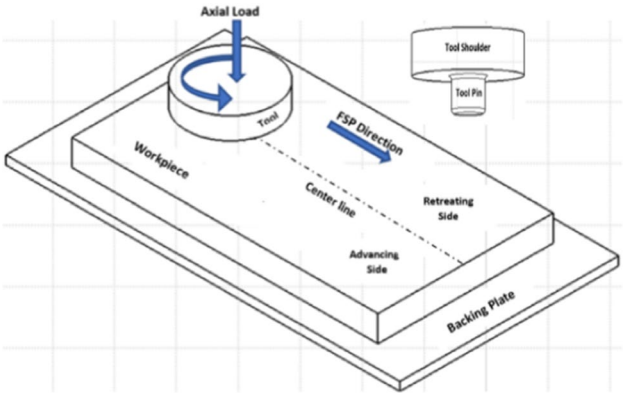

Fig. 1 Schematic of FSP

the heated material after it has flowed around the spinning pin. So, it is reasonable to believe that the FSP procedure is a hot deformation method, and that hot deformation microstructural mechanisms may manifest themselves during the FSP procedure [11].

The most prominent feature of FSP is the processing of workpieces without melting them and the plastic deformation of materials without external heating. Stirring phenomena in the process help refine grain, produce equiaxed grains, and enhance the base material's superplasticity [12]. FSP is also credited with improving microhardness, tensile strength, wear resistance, corrosion resistance, and other mechanical and surface characteristics. It has proven helpful in eliminating manufacturing and casting defects, repairing cracks, fabricating mono and hybrid composites, etc. [13]. Thus, many researchers used the FSP for microstructure modification and producing surface composites, using secondary phase particles (known as reinforcement) into the matrix with minimal greenhouse gas emissions, hence termed as green technology [14]. MMCs have wide-ranging applications in today's modern world, predominantly in transportation applications were the parent materials are replaced by composites Use of the FSP technique has been largely documented for improving the properties of cast aluminum alloys by surface modification [15], and MMC's in both ex-situ as well as in-situ routes [16]. Later with lightweight requirements, FSP found its applicability in magnesium and magnesium alloys for production of mono and hybrid surface composites [17], in improving superplasticity [18]. Moreover, Mg-based surface composites that are reinforced with fibers and particles can also be created by FSP. FSP makes it possible to produce magnesium alloys additively as a viable method for producing light metals [19].

FSP can be accomplished using vertical milling or by FSW machine. The microstructure of a processed material, which is normally controllable by changing process parameters, determines its features and the effectiveness of

the process. Process parameters must be chosen to supply the appropriate amount of heat to obtain the finest possible microstructure without any inherent faults. Various processed zone properties are the direct function of material flow, temperature, and particle distribution; however, the experimentation cannot provide a thorough insight during the actual FSP. Micro-to-nanoscale observation tools like the scanning electron microscope, spectroscopic characterization, X-ray diffraction, etc., are required for physical experimentation. Even these ultra-high-precision tools cannot monitor the physical quantities in real time and are limited to being used for post-process testing and examination.

FSP has gained significant attention for its potential to improve material properties. Still, the complex geometry and 3-D features of FSP make it challenging to analyze and optimize the process using experimental methods alone. Numerical modelling techniques have emerged as a promising alternative for simulating and analyzing FSP. However, numerical modelling is necessary to achieve an in-depth thermo-mechanical understanding of the FSP process, as it is challenging to understand the mechanics behind the process solely through experimentation. The complicated nature of the process involves several interconnected non-linear physical processes. It is characterized by enormous plastic deformation, mechanical mixing, frictional interface, dynamic structural development, material movement, and heat generation. The excellence of friction stir processed (FSPed) materials is also influenced by several process factors and the tool configuration. Developing governing equations for forecasting FSP behavior is complex as it comprises numerous process parameters, intricate shapes of geometry, and its 3-D nature. Furthermore, the mathematical formulation becomes exceedingly complicated due to non-linearity in material and plastic behavior, which is a big challenge to put together. Therefore, over the past decade, numerical analysis has been frequently used to address these challenges. While significant progress has been made in developing numerical modelling techniques for FSP, unanswered questions and challenges still need to be addressed. These include validating and calibrating numerical models, incorporating the impact of various material properties and parameters, overcoming limitations of different numerical modelling approaches, incorporating tool geometries and sizes, optimizing process parameters, accurately modelling the impact of frictional heating, and extending numerical modelling techniques to study FSP of advanced materials. Extraction of process temperature and material flow in the stir zone (SZ) during experimentation is complicated. Therefore, to obtain immeasurable data, there is a need to develop an advanced numerical model for analyzing the impact of various process parameters, multipass, and tool orientation changes on material flow which is currently in progress. Furthermore, surface composite thermo-mechanical models are needed to comprehend microstructure characteristics and analytical particle dispersion in FSP. This advanced comparative study with experiment may lead to productive results and offers a useful resource for individuals involved in FSW/FSP research and practice by presenting a practical manual for designing efficient processes for diverse materials. In general, it serves as a valuable reference for those seeking to enhance their knowledge of numerical modelling methods in FSW/P and their practical implementations.

Several scholars have examined the progress of FSP on aluminium and magnesium as materials for lightweight structures [20] and their mono and hybrid composites. FSW and FSP are discussed and reviewed by Mishra and Ma [21]. Zykova et al. [7] outline the most recent developments in the FSP of non-ferrous metal alloys, copper, and titanium. Patil et al. [22] and Bharti et al. [23] provided an exhaustive summary of the production of surface composites and a thorough understanding of the impact of process variables on the FSP operation. Additionally, researchers looked at several ways to reinforce FSPed hybrid surface composites and the effects of single-pass, multipass, and pass-direction variations on the microstructure and consequent properties [24].

He et al. [25] comprehensively reviewed the numerical study of FSW. The most significant parameters to study in FSP are temperature distribution and material flow. Nonetheless, measuring the temperature at the tool–workpiece contact during actual physical FSP is complex. Likewise, determining and monitoring flow patterns in materials is difficult. A wide range of trials can be carried out in numerical analysis by altering the variable, and a rare to the rarest environment can be created, which is very difficult to prove through physical experimentation.

Integration of numerical analysis with experimentation helps design, configure, and characterize the actual experiment to develop a more specific and optimum system economically. The numerical study of FSP involved solving a complex multi-physics problem associated with the visco-plastic flow of material, plastic deformation, heat flow, recovery, and recrystallization. State-of-the-art computers have reported a revolution in the field of modelling and simulation. Developing a 3-D model with the help of an advanced graphical user interface enables a more accurate and precise numerical analysis. Several researchers have developed the thermo-mechanical model for FSP with experimental validation and have obtained optimum parameters to achieve defect-free and significant improvement in properties. To the extent of the writer's knowledge, no comprehensive overview of various numerical techniques in FSP has yet been published. The main objective of this review is to outline the current research on the advances in the computational analysis of FSP, including the flow of material, the impact of process factors, the distribution of temperature, and heat

generation. The study also epitomized important numerical issues such as different modelling techniques, particle tracking, and challenges in computational analysis. The main methods, techniques, and approaches are reviewed in a brief study. Critical challenges and issues regarding the numerical study of friction stir processing remain to be solved, and opportunities for future research prospects are addressed.

The insights provided by the current study can have practical applications, primarily in industries including aerospace, automotive, marine, and energy. In the aerospace industry, FSP is used to improve the fatigue life of aircraft structures, reduce weight, and improve damage tolerance. Practical testing of FSP in the marine, nuclear, and aerospace industries is difficult due to the complex geometry of FSP and the 3-D features of the structures being tested. However, by choosing appropriate numerical techniques and assigning material properties, conditions, and constraints from the current study, researchers can gain insights into the behavior of FSP in these industries. In the automotive industry, FSW/P joins dissimilar materials, repairs damaged components and improve mechanical properties. The marine industry employs FSP to join and repair marine structures such as ship hulls and propellers, while the energy industry uses FSP to fabricate and repair components used in nuclear, oil, and gas industries. The study's insights can help in designing optimized FSP processes for different materials used in these industries, leading to improved durability, reduced weight, improved structural integrity, enhanced fuel efficiency, and reduced maintenance costs.

2 Different modelling techniques in FSP

Several approaches may be employed to imitate the different output results, such as temperature distribution and heat generation [26], material flow [27], 3-D plastic flow [28], coupled thermo-mechanical analysis [29], particle tracking [30], prediction of defects [31], heat transfer phenomenon of TIG processed sample with post-processed FSP [32], etc., to analyze the factual FSP/FSW process, including FEM and FDM. The temporal level investigates the influence of processing parameters, contact mechanisms/type (coefficient of friction), and thermal action in a specific zone; while performing a spatial level, it analysis the distortion, associated residual stresses, and overall structural temperature. The primary and derived numerical methods were proposed to investigate the behavior of the process at different spatial and temporal degrees, viz., Lagrangian, Eulerian and Arbitrary Lagrangian–Eulerian (ALE), CEL and SPH, respectively.

2.1 Primary numerical approaches

2.1.1 Lagrangian method

In Lagrangian groups, nodes and elements could distort and migrate in response to material deformation [33]. The Lagrangian approach is only employed for demonstrating thermal behavior across the entire texture and for minor mesh distortion issues, for instance, problems associated with invariable conditions. Element boundaries continue to coincide with boundary and material interfaces in Lagrangian meshes. Since governing equations are always assessed at the same material points, their computation is uncomplicated since the material points and the points at which outcomes are computed get coincides. A Lagrangian analysis is thus perfect for processes or solid mechanics with little deformation [34]. Owing to the high-level deformation of material during the FSP, the simulation suffers from significant mesh distortion where the traditional FEM-based Lagrangian technique cannot sustain it. A finite element simulation model was developed with coupled heat transfer model using DEFORM 3D based on Lagrangian formulation. To solve discrete governing equations and determine field variables, the conjugate gradient solver and the direct iteration approach were used. The modelling and simulation of friction stir tools with analytical models calculated the magnitude of forces operating on the tool [35]. With non-symmetric behavior and modified Lagrangian formulation, the friction contact produced between the tool shoulder and the base material has a friction co-efficient of 0.42. The tool shoulder and pin tip of the taper pin attained the most force during the plunging phase, while the pin side attributed the most force during the travelling phase.

For the processing of steels, a 3D Lagrangian implicit, coupled, a rigid visco-plastic continuum-based model was presented [36]. At different process variables, the model may be utilized to forecast temperature, strain, and strain rate distribution, along with thermal and mechanical stresses on the tool. A 3D Lagrangian implicit, coupled, rigid-viscoplastic, continuum-based FE model for the FSW process was put out [37]. To explore the distribution of temperature and strain in the heat HAZ and the SZ, the model was calibrated by comparing the output with actual data of force and temperature distribution. The non-symmetrical character of the FSW process and the correlations between tool forces and parameter change were appropriately predicted by the model. The FE approach based on a complete Lagrangian formulation was used to numerically investigate the evolution of ductile damage in an FSW aluminium joint exposed to stress [38]. An elastic-viscoplastic constitutive relation was used to explain the formation and expansion of micro voids. The authors coupled the simulation and mathematical modelling results of the temperature, which were utilized to build a statistical

model [39]. These techniques help to identify and predict the relation between the peak temperature and shoulder diameter, the tool's spinning, and linear speed.

To forecast the microstructure, the established model based on the Lagrangian approach was further expanded. Different pin shapes, including cylindrical [40] and square [41] pins, were employed to predict the formed microstructure during FSW/P using cellular automata. The growth of grain size was calculated using a less complex technique based on the Zener–Hollomon parameter [30].

2.1.2 Eulerian method

The nodes and elements remain steady in the Eulerian approach, allowing the material to transit throughout the domain [42]; the Eulerian formulations, on the other hand, are far better at dealing with material flow and are rarely used for modelling thermal behavior. This method's primary shortcoming is its difficulties in modelling free boundary surfaces because the boundary nodes may not coincide with the element nodes. As a result, it can only be applied when the deformed surface's boundaries are known in advance [43]. According to the researchers, it was rarely employed for specific thermal problems, unlike the Lagrangian technique, since it has a fixed mesh and allows the material to flow within boundaries. Bastier et al. [44] explained the use of Eulerian for hydrodynamic modelling and, with coupled approaches, can be extended to thermo-mechanical analysis. As a result, the Eulerian setup was frequently utilized in processes like fluid mechanics issues where the material moves through the grid. Additionally, the Eulerian formulation's application space is constrained since it necessitates a correct description of the convection term, material characteristics, and component shape [45]. In the FSW/P process, the Eulerian framework was mostly used by researchers with interlinked formalism. Cho et al. [46] initially used 2D Eulerian FEM for the texture evolution in stainless steel. Later they employed modified Petrov–Galerkin to the Eulerian Formulation technique for strain hardening modelling coupled with the visco-plastic flow and heat transfer in 3-D [47]. Under steady-state conditions, the Eulerian FVM approach was used by Cho et al. [48]. However, neither the transient temperature nor the impact of temperature on viscosity was considered in the model. As a result, it was revealed that there was a significant discrepancy between the numerical model's predictions and those of the temperature trials.

Feulvarch et al. [49] proposed modified mesh composition Eulerian technique for moving mesh. They split the mesh into two sub-parts: fixed around SZ and the base workpiece material as a second that moves with a solid circular motion with tool velocity. As a result, there were no mesh distortions, and the Eulerian formalism resulted in a satisfying computing time. Parallelly, a steady-state model was developed and split the simulation into two phases [44]. The pin motion was modelled in the first stage using the Eulerian formulation and re-meshing approach. In the latter, a steady-state approach was utilized to predict the residual stress based on an elasto visco-plastic constitutive equation. Recently, the Eulerian domain was employed to investigate the effect of tool tilt angle on thermo-mechanical behavior [50]. Symmetric temperature history was observed without a tilt angle; however, with a tilt angle, the T_p point shifts to the rear side of the tool, indicating good material bonding. Table 1 shows the Lagrangian and Eulerian techniques used by various researchers.

2.2 Derived numerical approaches

2.2.1 Arbitrary Lagrangian–Eulerian method

Both the Eulerian and Lagrangian approaches have upsides and downsides. The most viable technique for modelling big plastic deformation problems is to combine Lagrangian and Eulerian methods [51]. To preserve the good quality mesh with high strain rates near the FSP tool, ALE is used throughout the computation. ALE formulation in which the nodes can be programmed to move arbitrarily. The nodes on the boundaries are moved on the boundaries themselves, while the interior nodes are moved to minimize mesh deformation [52]. In comparison to the Lagrangian technique, the flexibility of moving mesh enables bigger indefinite distortions to be managed. Nevertheless, mesh motions have certain limits, making it challenging to manage extremely massive deformation. The difference can be clearly observed in Fig. 2.

$$\sigma = (A + B\varepsilon^n)\left[1 + C\ln\left(1 + \frac{\dot{\varepsilon}}{\dot{\varepsilon}_0}\right)\right]\left(1 - \left[\frac{T - T_{\text{room}}}{T_{\text{melt}} - T_{\text{room}}}\right]^m\right). \tag{1}$$

To study the impact of shoulder size on material deformations and the process temperature, three distinct sizes of the shoulder were employed to examine the temperature and equivalent plastic rate [53]. It was cleared from the modelling that; the maximum temperature is proportional to the size of the shoulder. The Power (P) required in kW for the process is the direct function of SD in mm and is given by Eq. (2).

$$P = 0.0156D^2 - 0.3483D + 3.215. \tag{2}$$

Their study notes that as the shoulder diameter rises, the temperature and material deformation in the SZ increases. Using quadratic polynomial approximation, the relation between the SD (mm) and maximum temperature ($T_{\max}$ in °C) can be expressed as

Table 1 An overview of Lagrangian and Eulerian techniques used in FSW/P

References	Base material	Approach/simulation tool	Objective	Outcomes
Bagheri et al. [55]	AZ91	Lagrangian–Abaqus Explicit	Small hole drilling analysis on FSP and vibration-assisted FSP (FSVP)	Higher deformation in SZ of FSVP compared to FSP Chip formation and its morphology: Discontinuous chips in FSVP with high hardness than the FSP Cutting force reduced in FSP
Chen et al. [56]	–	Lagrangian/–	Thermal history, stress analysis and forces involved during the process	Parametric study on stress and force distribution Reasonable agreement between experimental and simulation for temperature and force
Chenot and Massoni, Buffa et al. [37, 57, 58]	AA7075	Lagrangian-Deform 3D	To develop a model for thermal analysis	Lagrangian was discovered to be an effective technique for researching thermo-mechanics (temperature, strain, strain rate, forces, and material flow)
Ritti and Bhat [35]	Mg alloy; Tool-H13	Lagrangian-ANSYS	FSP tool design and simulation for Mg alloy	Low stress, long fatigue life, and little deformation were the results of the structural and fatigue examination of the tool Numerical analysis revealed that the tool is able to produce sufficient plastic deformation
Khandkar et al. [59]	AA2024; 6061 and SS304L	Lagrangian/–	Residual stress and Mechanical behavior	For obtaining multiple responses from the thermal analysis, Lagrangian was determined to be a suitable technique Analyzed the stresses; longitudinal stress was found to be higher
Jain et al. [60]	AA2024	Lagrangian-Deform 3D	Study of different solvers and adaptive remeshing on mesh distortion	Sparse solver together with sparse and conjugate combo found suitable Material around the pin was displaced by a single pin diameter in a circular path Remeshing tackled the mesh distortion issue
Gok and Aydin [61]	AZ31	Lagrangian-Deform 3D	Process parameter effects on temperature and strain for threaded cylindrical pin	Good agreement between experimental and simulation at 1964 rpm and 20 mm/min Effective contact by sliding-sticking in view of temperatures
Cho et al. [46, 47]	SS-304	Eulerian/–	2D and 3D models for texture evolution and strain hardening	Temperature distribution influenced by advection Texture evolution from computed velocity and hardening equation integrated with streamlines of flow Stain hardening using scalar state variables
Feulvarch et al. [49]	AA7075	Eulerian/–	To develop a 3D thermo-fluid flow for intricate tool shapes	Moving mesh technique avoids mesh distortions Material flow aspects need attention to treat all possible tool geometries

Table 1 (continued)

References	Base material	Approach/simulation tool	Objective	Outcomes
Colegrove et al. [62, 63]	AA7075-T6	Eulerian-CFD FLUENT	Temperature and material flow triflute and trivex pin in 2D and 3D model	Trivex predicted lower forces whereas triflute with augering action of material movement Heat input and strength did not vary much
Contuzzi et al. [64]	AA5754-H111	Eulerian-ANSYS	To predict the heat flux evolution in the presence of backing and clamping	The heating and cooling phases of treated materials were predicted by the model The cooling phase errors were at their highest and decreased with process speed Clamping did not affect the temperature profiles
Miles et al. [65]	SS304L	Eulerian-Forge	Prediction of grains from flow stresses, strain rate and temperature	Estimated the recrystallized grains in the SZ using simulated temperatures Grain size and hardness were just off by 10%; thus obtained model is favourable
Ren et al. [66]	AA2024	Eulerian-ABAQUS	Plastic material flow and temperature field in crack repair	The measured temperature reveals that the crack healing was in the solid phase Strength of repaired zone was restored with refined grains Chaotic material flow in RS and regular in AS
Bellala et al. [67]	AA7075	Eulerian and SPH (ANSYS an Altair)	To compare the accuracy of Eulerian and SPH techniques for thermal modelling in FSW	SPH was found to be a more suitable approach due to excessive mesh distortion The results validate the accuracy of the modelling techniques and provide insights into the temperature distribution and process parameters affecting FSW

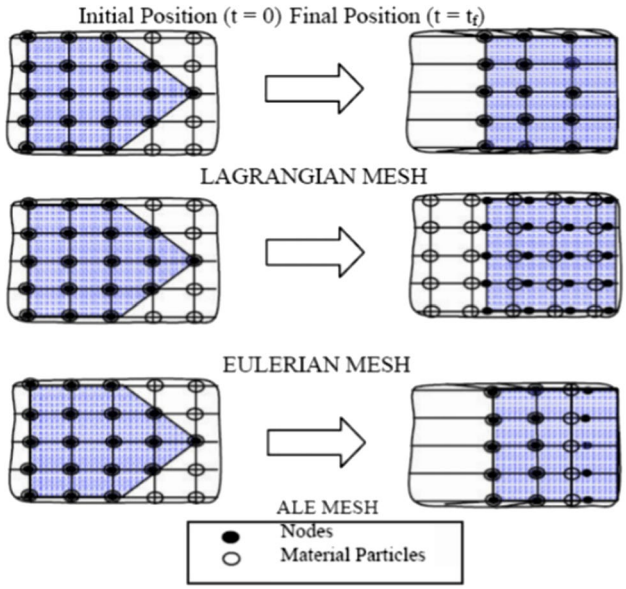

Fig. 2 The difference in the Lagrangian, Eulerian and ALE methods [51]

$$T_{\max} = -0.4437D^2 + 24.875D + 28.9 \tag{3}$$

Moreover, as the shoulder size increases, there is a significant refinement of grain size and homogeneity according to the recrystallization formula [54],

$$D_g = C \in^k \dot{\in}^j D_0^h \exp\left(-\frac{Q}{RT}\right), \tag{4}$$

where D_g is the average grain size because of dynamic recrystallization. $\in$ is the equivalent plastic strain and $\dot{\in}$ the strain rate. Q is the activation energy, R is the gas constant, and T is the temperature. D_0 represents the initial grain size. C, k, j, and h are constants, and k, j, and h are usually negative constants.

Researchers extended the application of ALE with tracer particles to evaluate the material modelling and transition [68]. In the stirring zone, a sliding mesh that rotates together with the pin (ALE formulation) may be employed to prevent very significant mesh distortions while keeping the remainder of the sheet's mesh stationary (Eulerian formulation) [69]. The material movement generated by the threaded tool pin was captured using a dynamic mesh technique that included both Lagrangian and Eulerian formulations. The developed 3D transient model tracks a threaded pin's translational and rotational motion [70]. The threads have only a little influence on the heat distribution in areas far from the tool pin. The fact is that current fluid-flow-based models ignore the material's elastic deformation when compressed.

This may cause considerable differences between expected and simulated values. Although thermo-mechanical models are well developed and employ advanced formulations, they cannot predict stress or monitor particle abundance throughout multiple segments. Fashami et al. [31] also used ALE with automatic re-meshing to process the AZ91 and predicted defects, thermal distribution, and peak temperatures. The Johnson–Cook model (JC) has been extensively employed for FSW/FSP because it accounts for temperature, strain, and strain rate and is shown in Eq. (1). With the help of this linked ALE and material model, they obtained the defect-free range of optimal process parameters. The rapid processing speed resulted in flaws such as tunnels and channels. In contrast, the minimal processing speed conditions generated high heat and caused defects such as flashes. However, the authors have not predicted the effect of low and high heat-induced defects on material flow. As a result, several researchers concluded that maintaining control over the TRS and TTS is essential for producing defect-free, more refined grains with higher mechanical characteristics at the end of the FSP.

The same modelling techniques were utilized for the multi-pass FSP to prevent mesh distortion during the subsequent passes with 50% overlapping. The results showed significant improvements in microhardness, tensile strength, and creep resistance, with a 3D model developed to simulate the process and study the temperature and residual stress fields [71]. Agha et al. conducted a multipass study on AZ91 light magnesium alloy using ABAQUS/Explicit to simulate FSP. The model incorporates Johnson-Cook models to define material behavior and a technique to prevent damage during processing, providing insights into the effect of process parameters on thermal evolution and stress distribution [72]. It was observed that the material behavior significantly affects the results of a developed simulation model.

The 2D and 3D simulation model was formulated based on the ALE technique using ANSYS/Fluent for 2017 AA. The material flow was not symmetric around the processing line, according to the 2D simulation. With the wider scope of ALE, the authors used a 3D simulation with the complete tool geometry and revealed the unique feature that the material flows around the pin and exhibits a centrifugal form. The material stirred on the advancing side rotates around the tool many times. In the thickness direction, the up-and-down movement of the material was also noticed [73]. At elevated temperatures, numerical analysis of cladding of similar aluminium alloys developed by ALE remeshing. However, the remeshing in future must be excluded to save computational time without compromising the accuracy of the model.

2.2.2 Coupled Eulerian–Lagrangian method

For commercial processes, the CEL model will be a powerful numerical weapon for simulating complicated thermo-mechanical processes and optimizing FSP process variables.

The CEL approach is an additional effort to combine the benefits of the Eulerian and Lagrangian methods. This technique is applied to fluid–structure interaction analysis (FSI) that involves significant deformation. In this procedure, the moving or solid structure is discretized using a Lagrangian frame, while the fluid domain is discretized using an Eulerian frame. The boundary of the Lagrangian domain is used as a guide for representing various domains. The velocity of the Lagrangian boundary serves as a kinematic constraint in the Eulerian calculation, defining the contact interface between the two components [74].

Vaira et al. [39] analyzed the impact of TRS and TTS on AZ91 magnesium alloy and validated a numerical model for the experimental results obtained from the literature. The highest T_p value of 916.84 K was obtained for a maximum of 1300 rpm and a minimum traverse speed of 0.5 mm/s. It was concluded that the T_p is proportional to TRS and negatively related to the TTS, as shown in Fig. 3, which is consistent with the research conducted by Adetunla et al. [75]. However, the built model does not predict the consequence of speed parameters and the temperature-dependent frictional coefficient on the plastic strain and T_p. Later, Ansari et al. [76] overcame the limitations and developed the numerical model using ABAQUS/Explicit based on CEL formulation for plastic strain distribution and varying coefficient of friction with respect to temperature. The developed computation-efficient process captured the T_p at four different rotational speeds with constant plunging and traverse speed on AA5083 aluminium alloy. For varied rotational speeds, the authors compared the measured and simulated temperature values at a site 4 mm offset from the centre axis on the AS. Increasing friction at the tool–workpiece interface produces more heat at higher rotational speeds. Thus, the material softens faster, and less force is required to distort it, with a net gain in temperature and strain rate of 18% and 48%, respectively. Increasing the coefficient of friction, a rise in the T_p was observed. Temperature differences in the

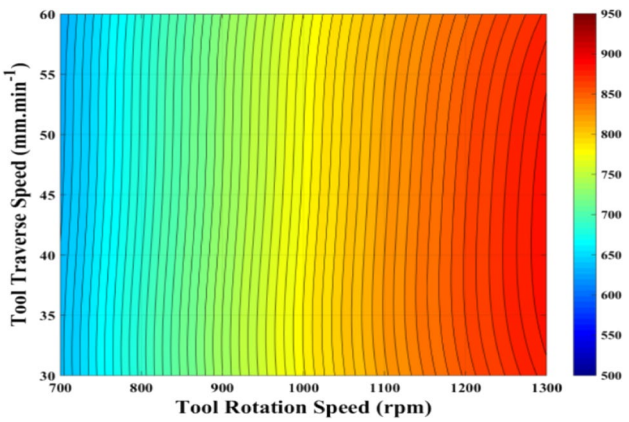

Fig. 3 Effect of TRS and TTS on peak temperature [39]

processed material are responsible for the corresponding plastic strain of the SZ, and it decreases as it moves deeper and further from the centre.

A blend of ALE, Eulerian, and Lagrangian descriptions is used in many computing domains known as apropos kinematic configuration. In this effective coupling method, the stir zone is treated as an ALE, the pin is treated as a Lagrangian formulation, and the remaining portion of the workpiece is treated as an Eulerian formulation [77]. Applying boundary conditions is made simpler by an apropos approach that allows for the effective treatment of any given pin geometries. It enables the treatment of random pin geometries and the practical application of boundary conditions. A mesh movement strategy used for the domain's ALE portion makes coupling with the other sub-Lagrangian and Eulerian domains easier [78]. Both frictional heating and viscous dissipation of heat were taken into account. The simulation's outcomes utilizing the suggested model were contrasted with the experimental data. Analysis was done on the impact of the slide and stick condition on non-circular pin shapes.

2.2.3 Smoothed particle hydrodynamics method

Gingold, Monaghan, and Lucy developed the SPH approach in 1977 to tackle problems in astrophysics [79], binary stars and stellar collisions, gas dynamics, and motion near black holes [80]. It is currently used in ballistics, volcanoes, seas [81], for multiphase flows [82] and later in various applications with random shaped boundaries [83]. With the advancement in SPH, it has become adaptable in the field of materials and manufacturing. SPH is modelled for mechanical analysis of brittle solids [84] and die casting process [85]. Lagrangian SPH may model the dynamics of interfaces, significant material deformations, and the material's temperature and strain histories without the need for intricate tracking systems. Recent research has suggested a newly smoothed particle hydrodynamics (SPH) model for FSW [86]. Simulations in three dimensions were performed on the AZ31 Mg alloy. Present were the temperature history and distribution, grain size, micro-hardness, and texture progression. It was discovered that numerical findings and experimental observations were in excellent accord. It is a new convenient mesh-free Lagrangian technique used to numerically identify the FSW/FSP behavior and is very well suited to large deformations. Since the method is Lagrangian, tracking the history of field variables at each node is naturally handled. The technique is particularly interesting for monitoring the free surface during the process. It allows for the inspection of the processed zone and defects such as lack of penetration, voids, and incomplete welds [87]. As a result, researchers are interested in using this technique to track materials subjected to enormous deformations and

strains. Fraser et al. [88] designed a thermo-SPH model coupled with the LS-DYNA program to implement the Johnson-Cook material model. Even though the model could forecast temperature, stress, and defect formation, their study did not determine the stress distribution and forces. Furthermore, the process's heat generation, temperature field, and stress distribution may be accurately predicted using the SPH. However, earlier analytical SPH research did not consider the stress, strain, and force factors to describe the FSW/P process effectively.

Ansari and Behnagh [89] implemented the SPH approach to analyze the plunging phase of FSW using ABAQUS/Explicit. The contact model for the tool and base material was defined by Coulomb's law of friction with a constant coefficient of friction (COF) of 0.5. The tool axial forces and stress-strain fields involved are predicted. The authors concluded that the force field, stress, and strain are all raised by increasing the tool penetration depth. Also, a direct relation was observed between the rotational speed, stress, corresponding plastic strain, and force. Experimental investigations leading to changing parameters from 600 to 1200 rpm increased the stress and corresponding plastic strain by around 3% and 19%, respectively, while the force was reduced by 22%. SPH being the time-consuming technique, the 25 × mass scaling helps in reducing CPU time. Even though the model was created for the plunging phase of AA6082-T651 alloy, it may be further used to investigate different materials and process phases. Additionally, Meyghani et al. [90] compared the ALE and SPH methods together to identify the effects of process factors on peak temperatures. Both models were suited for large deformation. However, SPH gives a thorough run of material during the process in the form of particles as kernel interpolation. They also employed the SPH technique for FSW on AA 6061-T6 aluminium alloy using ABAQUS [91]. It has been observed that the T_p on the AS was higher than the RS. Moreover, the temperature distribution below the tool was found to be uneven due to frictional heat distribution and plasticization. Top in the SZ was observed to imitate a quasi-steady process which quickly subsided as the tool traversed across the weld bead. They also found that the welding stress on the AS is higher than that on the RS. Several papers published on different techniques are depicted in Fig. 4. As a relatively new computing technique, the SPH method requires further development to address critical issues that currently hinder its widespread adoption. SPHERIC members who have recognized SPH Grand Challenges have taken the initiative to lead this endeavour [92]. Figure 5 portrays the combined experimental and numerical study of various factors that leads to a validated numerical model with appropriate strategy and formulation techniques. The summary of ALE, CEL, Apropos and SPH methods used are tabulated in Table 2.

2.3 Simulation of composites in FSP

Traditional liquid-phase processing procedures to manufacture mono and hybrid composites lead to the production of brittle compounds that are unfavorable, which are

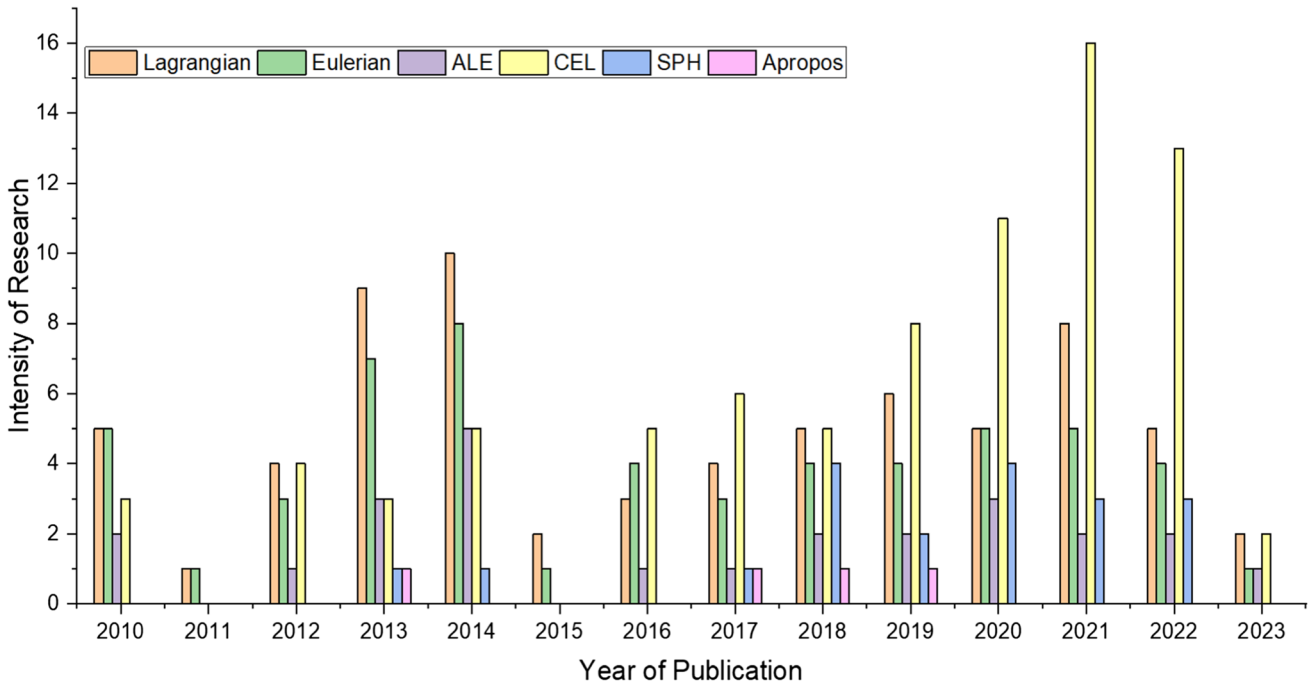

Fig. 4 Pervasiveness of the different modelling techniques for friction stir process in web of science

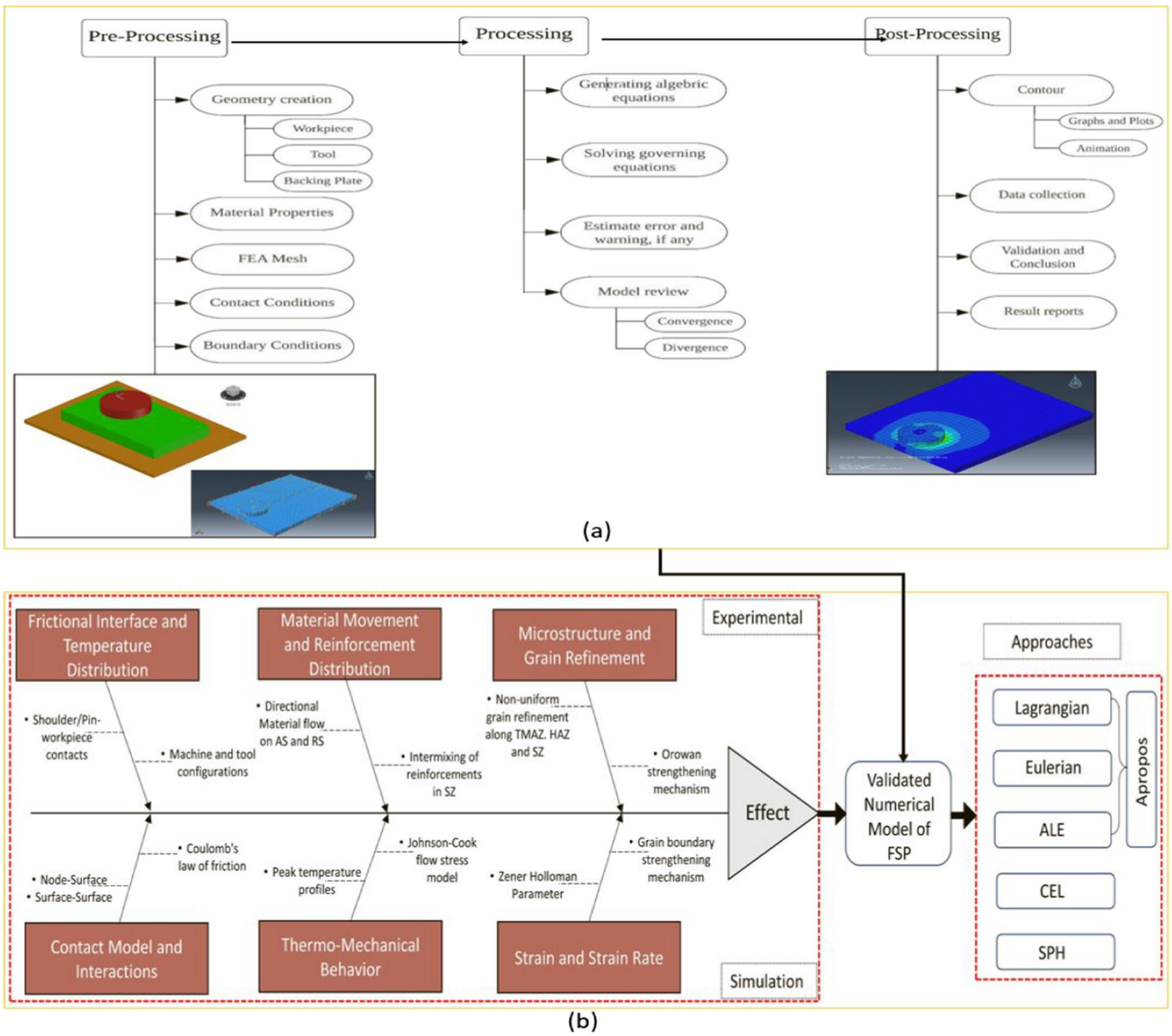

Fig. 5 Numerical model of FSP **a** implementation of basic strategy, **b** general validation steps involved with different approaches

destructive to the composite's final characteristics. FSP can be done with or without reinforcement, according to the requirements. Various researchers employed FSP to achieve superior material properties, and with further advancement, it has become the most sought practice for composites manufacturing. FSP makes a variety of composites: surface composites, where only the upper layer to a certain thickness of the base material is altered into a composite with no change to the base material, wherein in the case of a matrix composite, the entire material is changed into the composite. As a result, such transformation into composite demands many resources rendering it expensive. Surface composites have industrial applications in aircraft [93], marine, automotive [94], and military industries [95] for biomedical implants [96], where the material's desirable features solely depend on the surface. The numerical study of mono and hybrid composites helps in reducing the high cost of nano-reinforcement with resources and time. To forecast the types of defects, temperature profile, effective plastic strain, and flow of material in the SZ of LM13/Gr, a Lagrangian incremental model in DEFORM-3D was utilized [97].

The findings of material movements in the core towards the AS and RS were acquired by means of point tracking, where each point can be traced with the tool's movement. This technique can be used to analyze particle motion in hybrid composites. The tunnelling cavity and the slot behind the pin are shown in Fig. 6, mapped experimentally and computationally. The cumulative spinning speed and traverse speed being the same on AS, the SZ stretched on this high-velocity zone (AS). Uniform and smoother diffusion

Table 2 Summary of ALE, CEL and SPH methods used by several researchers

References	Base material	Approach/simulation tool	Objective	Findings
Bussetta et al. [98]	–	ALE/–	To compare the FSW with solid and fluid approaches	Both formulations delivered the same outputs of pressures and temperatures Fluid model is computationally more efficient. However, a solid model can be used to compute residual stresses
Dialami et al. [99]	–	ALE/–	Visualization of material flow in 2D and 3D models	2D model shows asymmetrical material movement at the processing line and no material mixing In the 3D model, the material is rotated around the pin more than once, and an up-and-down motion along the thickness of the material
Sallomi [100]	AA6061-T6	ALE/ABAQUS	Analyze temperature and strains in plunging, dwelling and traversing phases	Temperature was distributed symmetrically with V-shape in SZ after plunging Plastic strain was higher at AS Heat generation contributes to frictional dissipation energy
Saha and Biswas [101]	Inconel 718 alloy	ALE/ABAQUS	Prediction of temperature and stress	The workpiece produced identical temperature profiles; however, the temperature on the AS was a little bit higher Mechanical behavior was also investigated
Wang et al. [102]	AA5083	ALE/Deform 3D	Investigation of temperature and material flow on corner stationary shoulder-FSW	Elliptical profile followed by temperature, higher at the centre and lower at the periphery AS has a 43 °C higher temperature than RS The material in front of the pin flows with processing direction, whereas AS aS with the tool rotation
Mishin et al. [103]	AA6061-T6	ALE/Deform 3D	Predict the thermo-mechanical behavior of the two-stage deformation process (1st-tool pin and 2nd-shoulder edge)	The influence of TRS and TTS on temperature and strain was examined Higher temperature and effective strain were observed in the second stage
Dialami et al. [77]	AA6061	Apropos	To construct an ALE, Lagrangian, and Eulerian-based thermomechanical model	An obtained model is able to employ arbitrary pin geometries Predicted good accuracy in material flow
Dialami et al. [78]	Aluminium	Apropos-COMET	Investigate the impact of the pin on metal flow, torque and forces	The longitudinal forces are much greater than the transversal forces Two-stage simulation reduces 90% of simulation than the single stage When the pin shapes are changed, there is no obvious difference in the strain rate or stream-lines
Zhu et al. [104]	AA6061-T6	CEL-ABAQUS/Explicit	To develop a FEM model for the flawless processed zone	The size of voids was found to vary on the tool advancing rates The process has been intended to be optimized
Shamanian et al. [105]	Al-12% Si	CEL/–	Effect of process parameters on a temperature gradient	Temperature and plastic strain were directly proportional to TRS More heat is dispersed throughout the thickness, and less heat is created

Table 2 (continued)

References	Base material	Approach/simulation tool	Objective	Findings
Salih et al. [106]	AA6082-T6	CEL/ABAQUS	To examine how heat, plastic deformation, and residual stresses interact	Longitudinal residual stresses are higher than transverse TRS causes a rise in SZ's produced temperature and plastic deformation Enhances metal flowability, which lowers the number of flaws
Bhojwani [107]	AA6061-T6	SPH/LS Dyna	To develop a 2D SPH model for FSW	SPH yields the detail of deformation, stresses, and flow High strain at the wake of the tool 3D model, too, was developed and compared
Timesli et al. [108]	Aluminium alloy	SPH/CFD code	To develop an SPH model using the non-Newtonian fluid near tool of the FS process	Developed the first numerical SPH model CFD code The material flow was able to predict near the tool periphery
Yang [109]	AA6061-T6	SPH/LS-Dyna	To develop an additive FSP model using the mesh-free technique	Estimates were made for the temperature distribution, material deposition, deformation, and stress rate High hardness and stress were observed at the top deposition layer
Eivani et al. [110]	AZ91	SPH/ABAQUS and Neuro-fuzzy method	To develop an integrated SPH-neuro-fuzzy model	Residual stress was measured and compared with the numerical model (good agreement) This model can predict the influence of parameters on residual stresses and their sensitivity
Shishova et al. [111]	Aluminium	SPH/–	To understand bonding and contact mechanism (SPH-SPH) with compression and FSW process	Before the actual process, the bonding mechanism was implemented and studied using SPH Predicted bonding mechanism helps together with strength and contact mechanism
Marode et al. [112]	AZ91	SPH/ Altair RADIOSS	To develop a thermo-mechanical model and predict the in-process state variables during and after the process	Thermo-mechanical model successfully predicted temperature, material transition, and the emergence of a defect in FSPed material Wormhole defect was observed in FSPed AZ91 due to less induced pressure to fill the cavity of the pin at the rear side of the AS below the shoulder The lower compressive force was found to be a potential cause of the wormhole defect, suggesting the need for greater compressive force on the tool's backside to help diminish the flaw

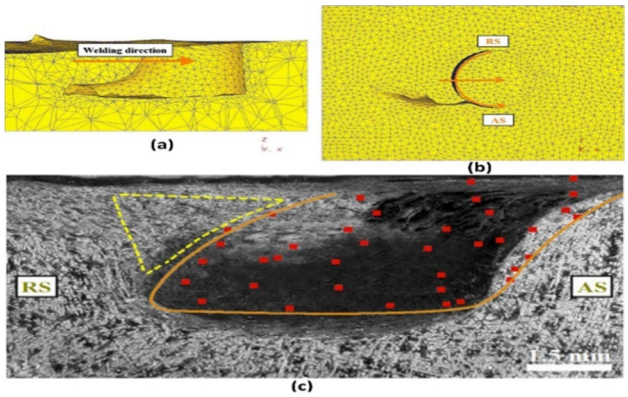

Fig. 6 **a** Tunnelling cavity formation at the behind of the pin and **b** slot formation at advancing side behind the pin. **c** Comparison of simulated and experimental SZ shape; Reprinted from Ref. [97]. Copyright 2012, Elsevier

of MWCNTs in the Polyamide 6 polymer was observed using ALE formulation [113]. The T_p appears as an unequal field at the tool/workpiece interface. Seven discrete points with 2 mm interspacing were marked on the surface of the workpiece, where three points were towards the AS, one on the centre line, with three, was towards the RS. It has been observed that, with the increase in the centre distance, the temperature at each discrete point decreases due to the direct influence of effective plastic strain and gap from the tool's centre. The results of point tracing support the form of the jug in cross-section in SZ. Modelling and simulation successfully predicted the thermomechanical properties of the Polyamide 6 with good agreement.

The impact of pin profile on the dissemination of B_4C in Al–Si alloy was predicted with threaded, circular, square, and hexagonal pin geometries examining the material transition in the process [114]. A three-dimensional thermomechanically linked FE model was used to numerically represent the material flow induced by the threaded and circular pins, which is the fundamental thought for particle dispersal in the metal matrix. A threaded pin provides vertical material movement, which does not exist in other pin profiles. Due to this reason, B_4C reinforcement particles were evenly dispersed in the SZ with the threaded pin, and the same was verified experimentally. Besides, they investigated the FSP of A356 matrix composites for the effect of reinforcement of TiC, SiC, B_4C, and SiC on mechanical properties, microstructure, and wear resistance [115]. The influence of pin geometry on the dispersion of reinforcing particles in the SZ was also studied. The homogeneous distribution of TiC with good bonding in the matrix observed in threaded pin profile same attributed by the simulation using DEFORM-3D. The hardness and grain size of as-cast AZ91 magnesium alloy doped with SiC nanoparticles was predicted by artificial neural networks using stirring speed, linear speed, and region type based on the amount of SiC particle in SZ [116]. The parametric impact of the inputs on the outputs is determined by sensitivity analysis. Linear regression analyses checked the adequacy of the model to calculate the correlation coefficients. Sensitivity analysis of the model outputs confirmed that the region types were the most significant element in the grain size and hardness of the manufactured nanocomposite. The data analysis was validated with the experiments. For the uniform distribution of reinforcement in the matrix and increasing the width of the SZ, an electric current was allowed to flow through the shoulder to the workpiece [117]. Numerical simulation was used to characterize the distribution of electric current density and the current flow and the consistent distribution of alumina fragments in AA5083-H111. Good bonding to the substrate was observed subsequently. The uniform particle distribution enhances the width and depth of reinforced tracks, allowing this study to diminish the number of passes and avoid having high rotating speeds.

Table 3 shows the variety of reinforcements used by many scholars in their simulation studies. Experimentally, it was observed that if the mono-reinforcement properties are insufficient for a particular application, hybrid reinforcement has been used, which gives a simultaneous property enhancement. Several researchers tested mono and hybrid reinforcements and concluded that hybrid reinforcements outperformed mono-reinforced composites in terms of various surface properties. The experimental optimization of process parameters is resource-intensive and time-consuming [94], but future research can optimize them more efficiently by considering numerical analysis. Additionally, the effect of process parameters on reinforcement volume percentage could be further investigated in future studies. However, compared to experimentation, very little work on simulation and modelling of mono and hybrid reinforcement composites has been done.

Way forward

- The numerical model for mono and hybrid reinforcements is yet to be studied.
- Although ALE can withstand distortion, applications involving heavy distortion need re-meshing or adaptive meshing techniques to counter the problem.
- Combined Eulerian–Lagrangian (CEL) get premature termination of computation and may influence the results.
- Advanced SPH framework must be explored for material movement and particle tracking.
- SPHriction-3D with GPU configuration must be investigated to dominate the computational time with simpler SPH techniques.

Table 3 Different reinforcement materials used in numerical research

Reference	Base material	Reinforcement	Approach/findings
Shojaeefard et al. [115]	A356	ZrO_2, B_4C, TiC and SiC	Material revolution around the threaded pin, a vertical material motion was observed Vertical motion discontinued the transverse bands formed in the cylindrical pin profile TiC achieved an increase in hardness due to excellent bonding
Shojaeefard et al. [114]	A356	B_4C	Studied different pin profile effects of the distribution of B_4C Compared to square, hexagonal, and cylindrical, particle distribution was almost uniform in threaded pin profiles
Tutunchilar et al. [97]	LM13	Gr	Lagrangian incremental FEM Material flow & SZ shape was successfully predicted Powder agglomeration and tunnel defects were observed at AS Microstructure and temperature rise matched experimental data well
Zinati et al. [113]	Polyamide 6	MWCNT	Arbitrary Lagrangian–Eulerian (ALE) The flow of materials and plastic strain T_p is observed at the shoulder/workpiece interface, and temperature distribution is asymmetric at the surface

3 Pre-requisite for finite element modelling of FSP

3.1 Material properties

Material information, properties, and their constitutive laws are the crucial elements of modelling and simulation to decide the accuracy and authenticity of the real-time process. During the FSW/P, the operating temperature varies from the ambient to the liquidus temperature of material as it is the elevated temperature deformation. Due to the distinct temperature zones in the FSP process, temperature-dependent material input data must be chosen to obtain a precise numerical model, and the same was endorsed by various researchers. It was estimated that during the FSW/P process, the higher range of temperatures and heavy plastics deformation with large strain ranging from 6 to 80, moderate to 5–100 s^{-1} high strain rate [34]. The constant temperature material data were often restricted to lower temperatures and plastic deformations [118]. Moreover, it was recognized that one of the most important input factors is the elastic modulus since a precise characterization of it can resolve the mesh distribution issue. It should have been highlighted that correct consideration must be given to other temperature-dependent factors such as thermal conductivity, thermal expansion, specific heat, density, yield, and tensile strengths [119]. Depending on the type of analysis, required and problem-dependent material properties are highlighted in Table 4. Materials friction coefficient also plays an important role in determining the accuracy of the numerical model. Localized softening lowers friction and the rate of heat production when the workpiece heats up. By changing the coefficient of friction, some researchers have taken this impact into consideration. However, there is no simple way to calculate the coefficient of friction or to determine how it varies with temperature or relative speed [120]. Frictional forces are shown to be responsible for 86% of the heat produced. Due to the fluctuation in temperature, strain rate, and stress, calculating the friction factor is a difficult task [121]. Because of the material's softening, which results in less solid roughness for the neighbouring material, it was believed that the friction coefficient would decrease as process temperature increased and thus influence the accuracy of temperature profiles [122].

Kuykendall et al. [123] investigated the effect of constitutive law on FSW model prediction and provided a guide for law. The authors put on hold the parameters and varied different laws and observed an up in temperature of 21%. Material laws are developed to be applicable to several physical scenarios, including isotropic elasticity, isotropic elastoplastic, composite and anisotropic, viscous, hydrodynamic, explosives, etc. JC material law is the most used model for characterizing the strain, strain rate, flow stress, and temperature history of the material. Depending on the type of analysis and application, the respective material must be chosen from the database of the FEA tools.

3.2 Finite element software packages

The choice of the finite element software package is a crucial step in the numerical modelling of the FSP. During the modelling of FSP, there are the certain aspect to keep in advance before selecting the FEA tool. ABAQUS, FLUENT, ANSYS, DEFORM 3D, and COMSOL-Multiphysics are some programs that are often used for modelling the FSP process [124]. Various commercially available finite element software packages have been briefly summarized in Table 5**,** along with information on how they may be used to

Table 4 FEA material properties (o-required and ↄ-problem dependent)

	Structural Analysis			Thermal Analysis		Coupled Structural-Thermal Analysis
Properties	Static	Dynamic	Fatigue	Static	Dynamic	
Elastic Modulus	o	o	o			o
Poisson's Ratio	o	o	o			o
Mass Density	ↄ	o	ↄ		o	o
Thermal Expansion Coefficient	ↄ	ↄ	ↄ			o
Thermal Conductivity				o	o	o
Specific Heat					o	o
Stress Strain Curve	ↄ	ↄ	ↄ			o
Fatigue Life Curves			o			o
Tensile Strength	o	o	o	o	o	o

perform FSP, including their individual potential with certain aspects. ABAQUS, ANSYS and DEFORM 3D are the industry standard for modelling mechanical characteristics, deformations, heat transfers, and temperature distributions. It was noted that FLUENT displays more precise accomplishments while modelling material flow and fluid dynamics [125]; however, the accuracy may differ from model to model. Therefore, a sophisticated FEA tool is required to construct an accurate and exact numerical model with complex structures and interactions. ALTAIR offers a wide variety of material data, property inputs and user flexibility to produce a high-precision numerical model in the FSW/P than others [126]. The limitation of computational time can be evaded by the hardware setting of GPU [127].

3.3 Type and size of the mesh

The fundamental tenet of FEA, which guides meshing, is to do calculations at a limited level of points and then extrapolate the outcomes over the whole domain of surface or volume. It is simply impossible to resolve the issue in this fashion since each continuous object has an endless number of degrees of freedom. The Finite Element Method uses nodes and elements to discretize or mesh to decrease the degrees of freedom from unlimited to finite. The mesh type and size have a significant impact on how accurate the simulated model is [128]. Based on the required accuracy and accessible computational resources, the type and number of elements are selected. One-dimensional: line or beam, two-dimensional: triangular or quadrilateral, or three-dimensional: tetrahedral or brick components can be selected depending on the modelling approach. Since the model for FSP is three-dimensional in nature, the quadrilateral or brick-type element shape is the most appropriate.

When results are post-processed, a coarser meshing decreases accuracy while a finer meshing increases processing costs. So, to ensure minimal results fluctuation and a reasonable model processing time, a balance between coarser and finer mesh must be reached. To do this, mesh convergence analysis must be performed to establish the optimal meshing size. For instance, a high level of modelling accuracy was attained when the FSW process was numerically and experimentally simulated with an element size of 0.3 mm [129]. Additionally, Kim et al. [130] chose an average mesh size of 0.1 mm close to the stir zone. It should be noted that the authors compared the results to the results of the experiments, and there was a good agreement.

The element size of 4 mm was employed distant from the welding seam to reduce time, whereas the size of 0.8 mm was used close to the heat-affected zone [131]. The mesh size was adjusted from 2.5 to 20 mm to examine the temperature distribution. When compared to the criteria outlined in the research, experimental measurements taken throughout the welding process demonstrated that the model's accuracy was adequate [132].

To conclude the overall mesh refinement research, FEA engineer should always opt for mesh size based on the intended output results because it alters according to the mesh sizing. To achieve a decent result with acceptable computational time, researchers should use mesh size of 1mm

Table 5 Distinct software packages and their potential

Aspects	ABAQUS	FLUENT	ANSYS	ALTAIR	DEFORM-3D	COMSOL-multiphysics
Geometric Modelling	Precisely supports 2D planar with shell, wire, and point. 3D; solid, shell, wire, and point	Builds 2D/3D control volume or domain for problem definition. Enclosure to fluid region Limitations in elements specialization	1D: beam, truss; 2D: Plane; 3D: solid, shell	1D, 2D, 3D, axisymmetric shell, thin shell, plate, membrane, axisymmetric solid	3D simulation allows the analysis of complex geometry, which cannot be accurately modelled using 2D	2D and 3D forms of modelling including shell & sweep without any addons
Distortions	Non-linear material model, multiple steps, contact analysis and other advanced techniques	Transient structure and high flow sustainability in fluids with contrary to solids	Explicit dynamic analysis, automatic remeshing, and quasi-static/gradual loading are preferable	Linear static analysis, Non-linear analysis, Non-linear quasi-static	Multiple deforming body capability allows for analysis. Body-to-body contact that is arbitrary facilitates the examination of many deforming bodies	Offers new moving mesh approach, free surface modelling feature addressing mesh distortions
Thermal Modelling	Heat generation, temperature distribution, and thermal stress analysis with transient and steady-state techniques	All three modes of heat transfer with material flow and multiphase change approach	Conduction, convection, transient thermal, static thermal analysis	Conduction, convection, radiation	Heat generation and thermal analysis. Capable of analyzing heat transfer and predicting large thermal behavior with astonishing behavior	Offers control over conjugate heat transfer, surface-surface-radiation, and Phase change, along with enhanced features
Material flow Modelling	Fluid flow stress, SPH and ALE techniques	More specific for fluid flows (steady, transient, 2D, 3D, streamlines, etc.) Constraint and limited solids	Turbulence modelling, single and multiphase flows, acoustics, combustion, conjugate heat transfer	Heat transfer, turbulence, non-Newtonian material analysis	Predict large deformation material flow with high precision	A dedicated model to simulate heat flow coupled with material flow provides better control over the process field variables
Adaptive Meshing ability	Limited accessibility, with precise control	Dynamic-moving meshing, Multiphase, Eulerian and Volume fluid model	Moving-mesh adaption, very coarse mesh and dynamically refined high-gradient regions	Provides users with the ability to create precise, high-quality surface meshes of their CAD geometry	Automatically applies an adaptive, optimized mesh to parts and tooling. User-defined and mesh customization	Supports adaptive meshing with a stationary or Eigen value solver/time-dependent solver
Material Library	Visco-elastic and plastic; hyper-elasticity and plasticity; isotropic and anisotropic elasticity; foam; with various sets of materials	Specific and individual fluid and solid materials. Global database, user-defined	There are more than 700 data sheets that describe the mechanical, electrical, and magnetic properties	Easy access to a wide variety of high-quality materials ready for simulation	Elastic, rigid plastic/viscoelastic, viscoplastic, elastoplastic, porous, hyperplastic, phases and mixtures, etc	Aided with many material domains, including piezoelectric and electromagnetic. Supports user-defined materials and the global database
Scaling	Focused towards quasi-static and supports dynamic analysis	Mesh scaling logs with domain extents	Automatic and easy in explicit analysis, increases the smallest time step and reduces the number of steps	Large extent to scaling without affecting the physics of the model. Avoid errors and infinite loops at a shorter computational time	Step scaling at local and global levels with customization. Limited to complex parts	Thermomechanical calibration provides a non-invasive calibration to the scaling aspect

Table 5 (continued)

Aspects	ABAQUS	FLUENT	ANSYS	ALTAIR	DEFORM-3D	COMSOL-multiphysics
Flexibility	Fine control in a process flow with tweaks required in solver functioning	Good accuracy and less computational time for less moving reference frames; solver gets complicated for more domains and higher frames	Offers APDL customization and solution for large-scale complex models	More inputs are required. Longer simulation time with high-end accuracy	Numerous processes are carried out automatically. Powerful post-processors are used to assess the outcomes of simulations. Display results graphically and can extract numerical data	Users can get high workability with modification in the solver interface

or 0.8 mm since the tool torque and temperature are mostly not depended on the mesh sizing. On the other hand, if a researcher intends to study the material flow/velocity and axial force on top of tool torque and temperature, then opting for mesh size of 0.6 mm is recommended.

Way forward

- There is still no indication that investigators are employing the mesh free-SPH method to simulate FSP numerically.
- To obtain macro to nano-level in numerical analysis of FSP and to achieve the high-end accuracy, application of ALTAIR is still scant.

Frictional contacts and interactions being the prominent feature of FSP, minimal studies were observed on the temperature dependent material properties with varying COF.

4 Thermal analysis of FSP

The heat produced by the FSP is mostly caused by plastic deformation and edge friction. To acquire knowledge on the temperature distribution during the FSP in light of the evident significant plastic deformation put to be difficult by the tool's rotation and translation action. The process's transient temperature field, maximum temperatures, active stress forces, and maybe even residual stress can all be predicted using thermomechanical modelling [133]. The physical connections between kinematics, heat transfer, high deformations, and strain rates in the treated zone surrounding the pin make modelling the FSP process just as difficult as simulating the FSW process. The material is significantly softened as a consequence of the enormous amount of heat that is produced in the FSP to boost the material's temperature. Rapid material flow and severe interfacial friction-induced plastic deformation are made possible by the material's thermal softening. Figure 7 depicts the coupling between the thermal and mechanical processes in FSP. The manner that heat is generated and, therefore, the temperature field are both impacted by the plastic flow of the material and the temperature change because of the close link between temperature and flow stress. The material softens due to the frictional heat created by relative motion at the tool–workpiece contact. As a result, the heat source is regarded as the workpiece surface that encountered the tool, and it comprises the shoulder bottom ($Q1$), pin side ($Q2$), and pin bottom ($Q3$) surface, as shown in Fig. 8.

$$Q_{\text{Total}} = (1-\alpha)Q_{\text{Sliding}} + \alpha Q_{\text{Sticking}}. \tag{5}$$

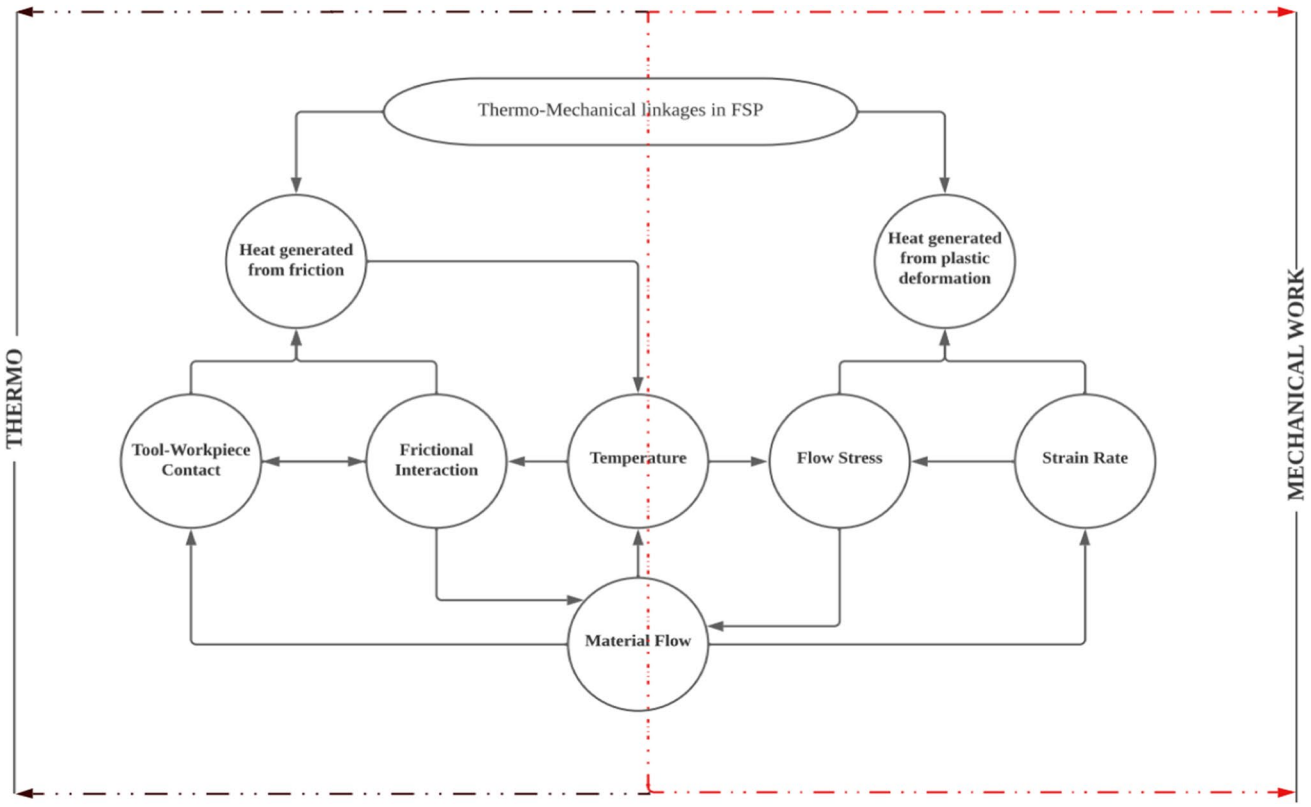

Fig. 7 Linkages between thermal and mechanical processes in FSP

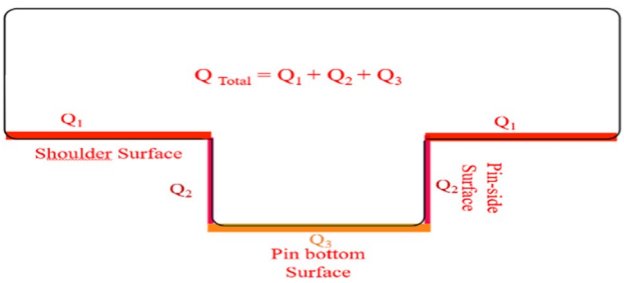

Fig. 8 Heat generation at different areas of FSP tool

The cumulative heat is given by Eq. (5), where α is the slip rate (dimensionless quantity), also known as the contact state parameter. The value of α varies when the friction mechanism at the contact surface changes. The range of α is in between $0 \leq \alpha \leq 1$, related to sliding when $\alpha = 0$, sticking when $\alpha = 1$ and partial sliding/sticking when $0 < \alpha < 1$ [134]. In another sense, when $\alpha = 0$, the only source of heat is friction. When $\alpha = 1$, material plastic deformation generates all heat. The significance of α is presented in Table 6. A three-dimensional thermal-assisted mechanical model was developed to understand the influence of speed ratio (TRS:TTS) on thermal distribution [31]. It was

Table 6 Significance of slip rate variable

Slip rate → Conditions↓	Range	Values	Heat generated
Sliding	0–1	0	Frictional
Sticking	0–1	1	Plastic deformation

noticed that with the rise in the TRS from 700 to 2000 rpm, T_p increased and reached 632 °C, as shown in Fig. 9.

The combination of TTS of 20 mm/min with 700 rpm and 2000 rpm produces adequate heat to cause the material flow, whereas, for more than 20 mm/min, the heat generated by deformations and contacts interaction was insufficient to allow for adequate material flow and complete material merging behind the tool. In addition, simulations on Al–12% Si Alloy disclosed the effect of TRS on temperature profiles [105]. Observations reveal that higher temperatures are produced in the vicinity of the tool–workpiece as the rotational speed was increased, and it is consistent with the findings of Kishta et al. [135], suggesting that due to the increase in the rotational speed, the strain rate, and plastic dissipation in the SZ increases, causing the workpiece to heat up more. Less heat is generated below the sheet, and more heat is dissipated to the backing plate. Thus, the elevated temperatures are all

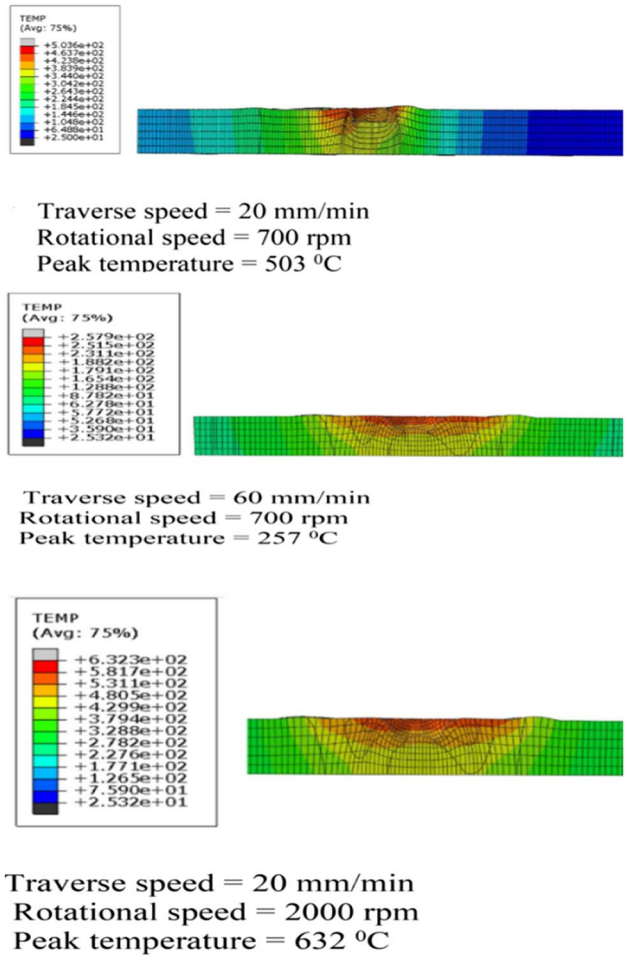

Fig. 9 T_p predicted at several process parameters for AZ91 [31]

the time found just below the tool shoulder and gradually decrease in the thickness direction. However, the models only reported the influence of process parameters on temperature and heat generated; the author did not account for the temperature and strain rate relation.

Post-process qualities of the material are studied with thermal distribution and strain rate as they were intensely affected due to the multipass [71]. A higher value of temperatures was observed at the interface of shoulder-magnesium plates and behind the pin following complete contact between the shoulder workpiece. Moreover, the temperature on AS was observed to be 24 °C higher than the RS due to the superior plastic deformation. As the stirring and travelling speeds are in the same direction, the cumulative effect stretches the SZ with a high strain rate towards the AS. A computational model was developed to predict the T_p of AZ91 alloy during the FSP [39]. According to the central composite design, TTS, TRS, and shoulder diameter were modified at five levels. Non-uniform boundary conditions for the upper side of the workpiece that undergoes FSP were defined because the temperature varies with time and process parameters. The friction factor, the interface area with the rotating speed, and tool shoulder pressure all contribute to frictional energy [136]. The temperature-dependent frictional factor has little effect on the processing temperature; therefore, the authors considered a constant frictional factor of 0.4 for the numerical analysis. Temperature distribution acquired on the surface and cross-section of the workpiece is presented in Fig. 10. The authors noticed that the non-symmetric distribution of temperature over the tool and elevated temperatures was towards the tool's tail. T_p of 387 °C and 452 °C at 5 mm away from the tool's centerline towards AS and on the rear side, respectively, was observed. Also, the

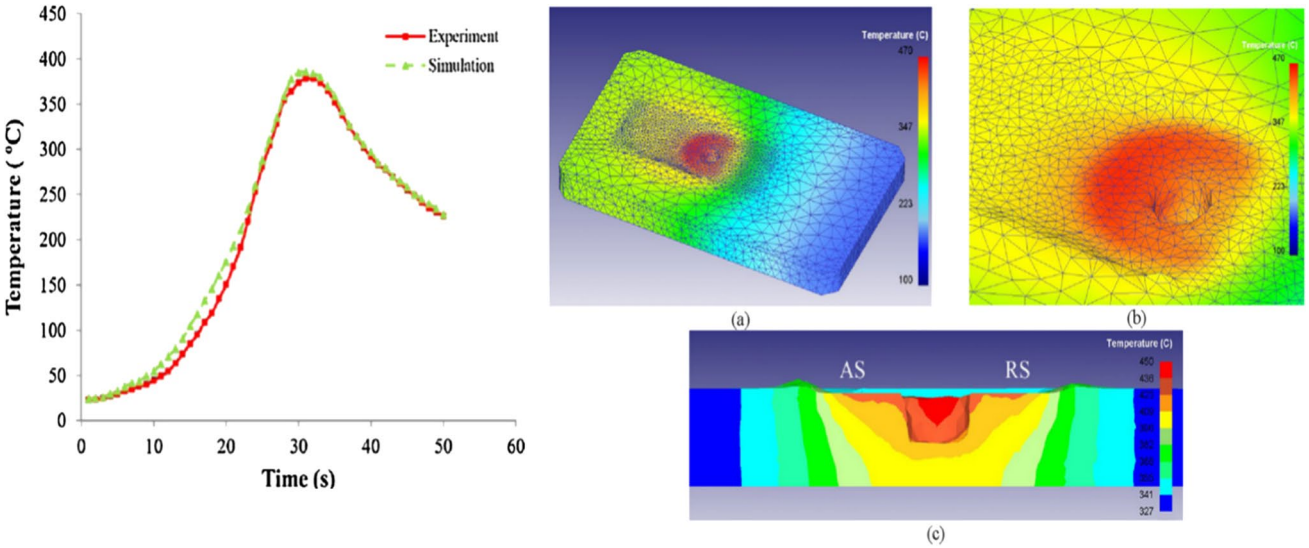

Fig. 10 Temperature profiles at SZ; **a** and **b** at the surface, and **c** at cross section; Reprinted from Ref. [136]. Copyright 2011, Elsevier

366 °C at a depth of 2 mm from the top and 5 mm from the centre. The figure shows the modelling and experimental temperature profiles obtained at 7.5 mm from the processing centre and is very consistent.

Thermo-mechanical outcomes of FSPed AZ31 alloy showed that rotating speed had a more significant impact on the thermal and strain rate than the translational velocity [137]. The analysis also reveals that the deformed material flow around the tool's centre resulted in a larger T_p and strain rate on the AS, whereas the material along the pin's path was wiped across the RS. CFD modelling was also utilized to tackle heat transport problems while considering the probability of liquid-phase production responding to the material to extreme heat in the processing. The temperature in the SZ rises as the rotating speed rises and falls slightly when the translational rate increases. Lowering the rotating speed, the temperature gradient increases substantially when the liquid phase occurs, and the highest temperature stagnates below the liquidus at high rotational speeds.

Excessive heat may be generated during the FSP of AZ31, resulting in aberrant grain development in the processed material [138]. On the other hand, repetitive high-temperature heating cycles can shorten the life of the FSP tool. The authors employed a 3D CFD model to examine the temperature effects of an internally cooled FSP tool. Reportedly, the highest temperature in the SZ was reduced by 75 K compared to the traditional tool, while the mean temperature of the tool body was reduced by approximately 200 K, which is expected to improve tool life.

Furthermore, when cooling is provided, the softness in the SZ and HAZ is lowered. Extending this study, in-process cooling during the FSP through the backing plate is provided and studied the effect on temperature fields using CFD analysis [139]. The width of HAZ was reduced by lowering the temperature values around the SZ through the channel geometry with a more extensive area inside the backing plate, which could help in lower grain growth and heat cycles after the process. Moreover, utilizing the low boiling point cryogenic fluids, such as liquid Nitrogen, at a high flow rate lowered the temperature by about 80 K under the pin zone, which helps to produce very fine grains. Cooling from the backing plate has only a modest influence on the shoulder interface heat, which is vital to simulate cooling strategies from the top surface to provide efficient cooling alternatives that envelop the entire sheet area. The temperature was reduced by roughly 80 K using liquid nitrogen instead of water and by around 20 K and 60 K by employing propylene and liquid argon, respectively. As manufacturing industries are progressing, innovative technologies like the additive FSP (AFSP) provide a novel approach to additive manufacturing. The filler or padding material can be dumped level by level on the substrate during this process, influenced by heat and deformation caused by friction between the filler rod and the substrate. A numerical simulation model [109] was created for perhaps the first film deposition using the SPH approach and applied LS-DYNA commercial tool to better understand the intricate physics of this advanced process. Their investigation unveiled the temperature distribution at different phases during the additive FSP on AA6061-T6 alloy. The entire HAZ was shaped like a bowl, and most of the heat was generated between the filler rod's contact surface and the substrate, then conveyed with the filler rod's movement owing to friction and plastic deformation. Due to the presence of material softening and pushing force by the filler rod, the maximum temperature reached 458.3 °C, which was ~ 79% of the melting point, at the circumferential contact surface of the filler and substrate.

On using two sets of process parameters, one with constant TTS and varying TRS and the other set with constant TRS and varying TTS, temperature distribution and heat generation were analyzed [140] using a 3D transient nonlinear model using ANSYS 11.0. In set 1, increasing TRS to 1000 rpm, the temperature rose to 683 °C because of the SZ's increased strain rate and plastic dissipation. However, in the la0ter set, higher TTS lowers the temperature as it allows for reduced processing time. Subsequently, the base material will have less chance to adhere to the material at high temperatures. Heat generation is substantially influenced by rotational and transverse speeds, where the T_p and heating rate are the strong functions of rotating and transverse speed, respectively. Thermal modelling helped to capture the temperature close to the tool's shoulder, and the difference is less than 15 °C compared to the experimental. Temperature changes were found to have a substantial impact on grain size. Al–Si alloy with Graphite was produced using FSP simulated with DEFORM 3D [97]. The temperature distribution obtained by simulation was compared with the experimental findings to validate the correctness of the simulation. Both simulated and experimental data were reported at 9 mm out from the processing centre on the AS and at 2 mm just below the top surface. Despite the numerical temperature values being somewhat higher (19 °C) than the experimental readings, the simulation results are reasonable and acceptable, following the actual data. To create repeatable, high-quality FSPed materials, a proper selection of processing parameters is required. These onerous objectives drive a numerical-experimental method to optimize processing parameters such as speed ratio and plunge depth to achieve effective grain refinement and uniform dispersion. Careful process parameter selection can guarantee that the processed zone receives enough heat to maintain acceptable material plasticity, but not so much that grain refinement is compromised. The relevance of the frictional coefficient in forecasting the temperature field in FSW/FSP is negligible for the slight changes in the frictional coefficient, even though the detailed numerical model with

temperature dependent frictional coefficient is needed. It should be emphasized that FSP is being investigated primarily as a way of causing extreme plastic deformation to homogenize and refine the material's microstructure without any inherent defects. The temperature and heat generation during the reinforcement is also of equal important to understand the thermo-mechanical behavior of nanoparticles and its consequence on matrix during the production of surface composites. However, research is still in progress for data in temperature fields, material flow and defects occurring due to reinforcement at various process parameters and their combinations for affective modelling and simulation of surface composites.

Way forward

- Temperature and heat generation with and without any reinforcement must be studied in future to compare their thermo-mechanical behavior.
- Researchers have analyzed various defects during the FSP; however, the relation between the temperature, strain, and strain rate with a type of defect is still in progress.
- The effect of temperature-dependent COF on MMCs must be explored to understand its effects on material softening.

5 Material flow modelling

A lot of research has been conducted to simulate the materials flow during FSW in addition to experimental methods utilizing various computer codes, basic geometrical models, metalworking models, boundary layer flow phenomenon [141] and mathematical modelling tools [142]. These efforts were made to comprehend the fundamental physics of the material flow that takes place during friction stir technology. Heat generation results from plastic deformation, and friction plays a crucial role in the material flow during FSW/FSP by regulating flow stress.

It is not sufficient to rely solely on visual inspection of defects without interpreting the material flow, as this only provides information about surface defects [143]. Therefore, numerical modelling can provide a more in-depth analysis. Memon et al. [144] studied the effects of PD during FSW of an Al–Mg–Si alloy T-joint were investigated using CFD simulation, and macrostructure visualization was used for joint evaluation. The study demonstrated that PD significantly affects material flow and defect formation in the joint. A recent study used the CEL formulation to investigate welding defect formation in AZ61 magnesium alloy using FSW. The 3D finite element model was validated with experimental results and utilized the modified Coulomb's friction law and temperature-dependent friction coefficient values to accurately predict weld defect formation and seam geometry [145]. These findings could be relevant to the development of numerical modelling techniques in FSP.

Material movement is a prime aspect of the FSP because it impacts the efficacy of the treated material. The plasticized material is delivered behind the tool on the RS, where most of the material movement occurs. The material flow around the tool is highly convoluted, and it is affected by the tool shape, several process factors, and the material to be processed itself. Understanding the material flow characteristics is crucial for the best tool design and process parameter combinations. Several numerical models of FSP have been built and discussed in this section to compute material movement. Thermo-mechanical modelling of FSP on AZ91 discovered that large material displacement, effective stain, and T_p can be obtained using conical pins by Hassanamraji et al. [146]. Pin structure affects the material flow severely in terms of pattern. A cylindrical pin causes particles to accumulate on the top surface towards AS. In conical, vortex flow downward avoids the accumulation of particles at the AS, contributing to the uniform distribution of particles. Larger displacements of material in conical would evolve a rise in the temperature compared to the cylindrical pin. To better understand the physics of material flow during FSP of magnesium alloy, Asadi et al. [136] used the point tracking method in DEFORM 3D. Points or nodes were located and tracked on AS and RS with the tool movement. The tool pin's purpose is to rotate the front material to the back and fill the void left behind during the transverse movement. Thus, nodes located on the AS adhered to the tool pin and moved towards the RS. Some particles from the AS entered the SZ and were stretched towards the AS. However, in the array of points, the upper few points experienced high displacement, and hence the points away from the shoulder may belong to the zone other than SZ (say TMAZ). In contrast to AS, points in the retreating site moved backwards and did not rotate with a pin. This was in line with the reported study by Zhang and Zhang [147] for the FSW. Although a large amount of strain is employed with RS, the authors did not observe the sign of mixing in the SZ and are supposed to belong to TMAZ. Due to the rapid plastic deformation and high cumulative output velocities with advancing movement, material shearing is typically moved more on the AS. In the same way, the point-tracking approach was utilized to simulate material flow for two different pin shapes: cylindrical and conical [146]. Using the tracking method, the authors predicted whether the material around the tool was symmetric or not. Due to the varying feed rates and speeds of the components on each side of the tool in AS compared to RS, the materials are exposed to increased displacement. If TRS and TTS are in the same direction, the output speeds are calculated by adding them. However, the output of speeds

may be calculated if their directions are reversed or opposite from one another by deducting the velocity component. This information demonstrates that the material particles on the RS are susceptible to two opposing flows, which increases material flow friction.

On the other hand, the material points on the AS travel were more smooth than the RS. As a result, the AS material was subjected to a prolonged flow regime and larger displacements. Similarly, using 3D transient Computational Fluid Dynamics (CFD), massless particles were implanted in the simulation domain of magnesium alloy to trace the detailed history of threaded pin material flow [70]. The authors observed three distinct flow zones in the model: the shoulder affected zone where the material was swirled strongly left to right around the tool shoulder and slightly forced descending in the typical route. The next zone is on the plate's bottom surface and on the RS, where the material was expelled for approximately half rotation (180°) in the vicinity of the pin. In the third zone, near the bottom surface of the plate as well as on the AS, the material was caught in stirring and rising flow pitch generated by the helical thread. Thus, the material can have a distinct thermomechanical history during FSP, reliant on its location. When the tool passes across the predefined set of points, the point-tracking approach helps get insight into the material movement [113]. The authors positioned 12 nodes at 0.5 mm increments at various depths from the top to bottom surface. Since the tool shoulder, coupled with the pin, accelerates material flow at the top surface, the first six points are turned towards the retreating zone with a bigger diameter than the tool-pin diameter, making the SZ wider cross-section on the top surface. The next four intermediate points rotated with a probe with the same diameter as the pin. The extreme bottom two points depict the flow pattern at the lower side of the SZ. The 11th point climbs upward to the surface, but point 12th moves very little. Material on the lower side of the pin flows upward to the stirred zone, but the material beneath was unaffected by the FSP.

Streamlines are a group of curves that are always tangent to the flow velocity vector. These depict the path that a massless fluid element will take at any given time. As demonstrated in the magnified view of Fig. 11 [137], the top surface in the inset flows from the AS to the RS, and the deformation zone on AS appears to be smaller. The pin site material is carried around the tool's RS. When tool slip was considered, similar material flow parameters were reported in several modelling surveys. However, it is worth noting that essential and crucial characteristics of material flow may be examined with a basic assumption of the full stick condition. The streamlines study shows the intensified activity behind the tool, likely indicating a large flow behind the AS. The width of flow lines shrinks as getting closer to the

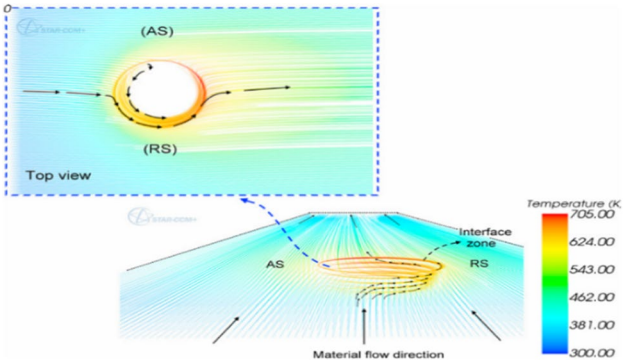

Fig. 11 Streamlines of material flow and temperature (TRS: 1000 rpm and TTS: 9 mm/s); Reprinted from Ref. [137]. Copyright 2013, Elsevier

shoulder, suggesting that flow is more robust in the material's higher layers.

Localized melting at the tool–workpiece interface could result from significant heating in the stirring region due to friction and extreme plastic deformation. To explore this, the partial melting concept was incorporated into the simulation to explore its understanding during the process. Nassar et al. [148] investigated flow velocities and material flow using the partial melting effect. They discovered that rotational flow velocities decrease as a semi-molten layer forms around the tool, inferring less shearing for microstructure refinement. This may result in abnormal grain growth and adversely affect the characteristics of the materials. Thus, the optimum process parameters must be chosen to avoid the unusual thermo-mechanical behavior of the material. The material flow was also monitored during the crack repairment of AA2024 aluminium alloy using FLUENT simulation [66]. The material flow in the vicinity of the shoulder is adjacent to the advancing direction, whereas, in the RS neighbourhood, it was mixed and chaotic. Furthermore, the flow velocities of the materials vary below the shoulder as it depends on frictional contacts. Moreover, the material farthest away from the shoulder centre has a higher velocity due to the increased circumferential speed.

Shoulder's spinning and swirling activities are substantially less for materials with 1mm below the upper surface of the specimen, resulting in a fall of flow velocities. Although most materials go downwards due to the shoulder's forging action, a few portions of the materials still have an upward movement inclination due to flow stress. In particular, plastic materials are preferred to flow toward the shoulder centre to fill the cracked gap, which leads to crack repair. Material flow takes place layer by layer, either lateral or linear, to the tool in the base material, irrespective of the process, which strongly influences the characteristics of the processed material.

Numerous researchers have worked on material transportation during the FSP; however, the comparative study of material flow for each pass and flow analysis of FSP with any secondary phase or reinforcement is still in the future scope. The study of material flow in the simulation of surface composites would be possible with an advanced SPH technique and efficient graphics processing unit, which reduces computation time [126]. Tool tilt angle is one of the crucial process parameters in deciding the amount of material to be rotated. The relative velocity is significantly affected by tool inclination, and the uncontacted area gets larger when either the stirring rate or processing speed increases [149]. Several authors claimed that by applying the tilt angle, the contact area between the tool and workpiece also rotates across the processing route (x-direction) [150]. Dialami et al. [151] found that the non-zero angle results in a decrease in material flow stress in the rear AS, facilitates the material flow behind the tool and strengthens the material stirring action at the trailing of AS. However, this rotation does not affect the geometry of the contact area. The rotational angle of the contact area with respect to processing direction is the β. The basic equation for material velocity is given by Eq. (6)

$$\text{Material flow velocity (m/s)} = \omega \times R, \tag{6}$$

where ω is tool rotational speed (rad/s), and R is shoulder radius (m). Therefore, with tool tilt angle (α), the velocity components of material flow in x (processing direction), y (plunging direction along the thickness of workpiece) and z directions (along the workpiece width) are as given below:

$$\omega_x = \omega \times R \times x \cos\alpha \times \sin\beta \tag{7}$$

$$\omega_y = \omega \times R \times \cos\beta \tag{8}$$

$$\omega_z = -\omega \times R \times \sin\alpha \times \sin\beta. \tag{9}$$

Way forward

- The physics of material flow during FSP is very convoluted, poorly understood, and needs more emphasis.
- Complete knowledge of material movement and deformation processes surrounding spinning tools is still lacking and is essential for optimizing FSP process parameters and designing tools.
- Material movement with the addition of a second phase is still an unexplored area that needs to study in the future to avoid manufacturing complexity and cost.

6 Challenges in numerical analysis

Due to the inherent computational challenges, addressing the complex non-linear and highly coupled physical phenomena through computational modelling and numerical analysis of FSW/P is a very challenging process to accomplish [152]. Several intricate elements have further complicated the numerical analysis of the FSP using FEM. Momentum and energy balance are governed by the same equivalent equations that explain the equations of the problem with a thermomechanical connection. The nonlinearity of the governing equations has a substantial influence on the numerical model's complexity. Therefore, a reliable and efficient numerical technique is in great demand to solve these highly nonlinear coupled FE equations. The process can be numerically simulated in either of the two methods, namely the Localized method and the global method [153]. HAZ of the simulated workpiece is the major priority in the case of Localized level analysis, where the investigation aims at deriving the heat power produced by friction at the contact phases or due to the visco-plastic dissipation. During this level, important process behaviors include the interplay of process variables and the contact mechanisms as they relate to normal pressure applied, coefficient of friction, setup geometry, the flow of material, material size, and formation of the associated microstructure, among other factors. In a global simulation, the whole component that will be FSPed is being studied [154]. The boundary condition that corresponds to the real HAZ at each time step is subjected to a dynamic heat power source. This kind of study focuses on how the processing line influences structural behavior such as aberrations, weaknesses or residual strains. The following six sections include the difficulties associated with the numerical modelling of the FSP process.

6.1 Thermo-mechanical problem

Numerical modelling applications have been expanded to the aerospace industry through the development of thermo-mechanical models, which minimize the need for experimental trials to determine the most effective process parameters [155]. The energy balance equation attempts to define the thermal component. In the Friction stir process, the energy equation and the plastic dissipation component play a major role during the process and serve as the primary source of internal heat [152]. One of the essential ideas in the effective numerical integration of the process is the specification of the heat source. It is often impossible to characterize the shape of a processing zone or a fluctuating heat source using the mesh size that

is used to define the model at the global level. However, the aim is only accomplished via local-level analysis. The size of the heat source does not match the typical element size for a thermo-mechanical analysis when the whole structure is taken into consideration.

Additionally, the final element size often is not fine enough to accurately reflect the real geometry of the heat source. The thermal governing equations may have a convective component according to the kinematic structure used in the linked thermo-mechanical model [69]. As a consequence, for convection-dominated issues, temperature instability due to convection developed [156]. It is good knowledge that issues with diffusion dominating have stable solutions. However, when convection is dominant, the stabilizing effect of the diffusion term is insufficient, and temperature field variations begin to emerge.

The momentum balance equation controls the mechanical issue. Due to the high viscosity characterization, it is possible to assume that the mechanical analysis will be quasi-static since the effects of inertia on the operations are minimal. The volumetric changes are determined to be insignificant at the local level, and incompressibility may be assumed. It may be very practical and advantageous to split the stress tensor into its deviatoric and volumetric components to cope with incompressible behavior. Mixed velocity-pressure interpolations must be used to deal with the incompressible limit. If suitable spaces for the pressure and velocity fields are not employed, the issue becomes unstable when the typical Galerkin FE formulation is used [157]. Thus, if the equivalent velocity-pressure interpolations are utilized, pressure instabilities show up. As a result, the difficult problem of pressure stabilization emerges. Extremely high strain rates and a large temperature range, from ambient to the melting point, are characteristics of the FSP process. Therefore, the constitutive rules that are approved should be based on both factors. The substantial strain deformation at conventional welding temperatures is mostly visco-plastic. Elasto-visco-plastic or rigid-visco-plastic impose conditions may be utilised, depending on the study's scope [158]. The goal of the FSP simulation is to accurately determine the residual stress field created throughout the procedure as well as to estimate the temperature progression. The chosen constitutive model must accurately describe the behavior of the material and be calibrated using temperature evolution. Due to these constitutive models' significant non-linear behavior, which presents a problem, a niche approach is required from a numerical perspective. The challenge is further complicated by the localized significant strain rates often encountered in the process.

6.2 Framework for kinematics

Making a proper kinematic framework for the modelling of FSP is a significant task. The problem may be described using a Lagrangian framework if the process is looked at on a large scale. The Lagrangian Frame of Reference makes it simple to observe interactions between various materials and free surfaces. The HAZ is the primary focus of a local simulation; therefore, a Lagrangian framework is not usually required. Frequent re-mesh would be necessary due to large distortions. The use of Eulerian or Arbitrary Lagrangian Eulerian (ALE) techniques is one option. Significant fluid motion distortions are simpler to manage using the Eulerian formulation. Its disadvantage is that it is difficult to monitor free surfaces and interactions between various media or materials. In flow problems with shifting and deforming borders, an arbitrary Lagrangian–Eulerian (ALE) formulation is quite useful. Providing an appropriate kinematic framework is crucial when modelling techniques for representing different components of a computational domain, such as setting up various zones or regions [77]. Although a framework that incorporates sliding mesh and pin with ALE formulation can address the issue of mesh distortion, it may have an impact on the model's accuracy, as discussed in reference [152]. Despite the concept's success, controlling the connection between the domains and the mesh movement approaches are challenging.

6.3 Frictional contact issue

The numerical analysis of FSW/FSP presents challenges as a result of the complex thermo-mechanical frictional interaction between the tool and the workpiece. Understanding the friction phenomenon remains a very scarce and challenging area in numerical studies. Assuming a constant friction coefficient can lead to a higher percentage of errors and inaccuracies in the analysis [159]. This assumed interaction can lead to temperature rise, incipient melting, and tool slippage, complicating the numerical modelling process. To overcome these challenges, one recommended approach is to use a friction coefficient that varies based on the surface temperature [160]. Additionally, temperature-dependent shear friction coefficients have been recently applied in refill friction stir spot welding to compensate for incipient melting and tool slippage during the process [161]. Implementing these two strategies can improve the accuracy of numerical analysis for FSW/FSP processes.

The simulation model must accurately account for thermal interaction at the surface of contact, heat generated by friction, frictional behavior, and impenetrability of contact [162]. The friction force and temperature pattern are directly controlled by the contact pressure, according to Zhang et al. [163], that compared the standard and modified Coulomb

friction models. To model the mechanical frictional contact interaction, direct elimination methods, Lagrange multipliers, Uzawa's version of the augmented Lagrangian approach, or penalty-based approaches such as the penalty method may be used. In the context of a fluid mechanics approach, the Norton thermo-frictional contact model may be used to compute the tangential component of the traction vector at the contact interface in terms of the change in the relative slip velocity. A portion of the heat flux generated by friction at the tool-to-workpiece contact interface is absorbed by the tool, while the remaining portion is absorbed by the workpiece. The amount of heat absorbed by the tool and the workpiece is dependent upon the thermal diffusivity of the two materials in contact. The worst-case scenario may also be considered to include full stick thermo-mechanical contact between the tool and the workpiece.

6.4 Coupled problem

A set of discrete nonlinear algebraic equations are created from an infinite dimensional transient system for the numerical resolution of the coupled thermo-mechanical problem [69]. This is accomplished by updating the internal variables of the constitutive equations, the FE spatial discretization method, and the time-marching scheme of the principal nodal variables. Using time-stepping systems, linked thermo-mechanical problems can be resolved in one of two ways. A monolithic (simultaneous) time-stepping method is the first choice; it simultaneously handles mechanical and thermal problems. Each of the key nodal variables in the problem is advanced at the same time. This strategy's key benefit is that it makes it possible for the linked issue to stabilize and converge as a whole. The time-step and time-stepping methods must be the same for all subproblems in simultaneous solution procedures, which may not be effective if the thermal and mechanical problems entail different time scales. Significant downsides include the requirement to develop software and solutions that are specific to each related circumstance and the monolithic algebraic system's extremely high processing complexity. Another option is to employ a staggered method that addresses the two subproblems one at a time (such as block-iterative or fractional-step). A staggered solution is offered by an operator split and a product formula approach, which often has a greater processing efficiency. Staggered solutions are produced using a connected set of nonlinear ordinary differential equations and the product formula approach. When used with conventional fractional step techniques, this operator split divides the original monolithic problem into two more manageable and well-conditioned subproblems. As a consequence, the main issue is divided into more manageable, usually symmetric (physical), sub-issues. The use of the various traditional time-stepping algorithms developed for the decoupled sub-problems and the use of the different time scales involved is then straightforward. The potential loss of precision and stability are these approaches' primary flaws. Therefore, it is possible to create unconditionally stable schemes using this approach if the operator split maintains the underlying dissipative nature of the original problem.

6.5 Particle tracking

One of the primary concerns with FSP's local research is the production of heat. It takes a significant amount of heat for the material to move and undergo a dramatic material shift. Due to the material not being adequately softened to flow, voids develop when there is a lack of heat. Visualizing the material flow is quite beneficial for better understanding its behavior. But either physically (needs metallographic tools) or statistically, it is difficult to follow the location of the material during the procedure. Creating a numerical approach for visualizing the material trajectory to understand and track material penetration inside the thickness of the workpiece is one of the key challenges of numerical simulation. The method known as particle tracing effectively replicates the mobility of material points by keeping track of their positions at each analysis time step [164]. The displacement field defines the trajectories in the Lagrangian framework. Both the Eulerian and the ALE frameworks take some time to indicate where the material is in the solution. However, by integrating the velocity field, it is possible to determine how much material mixing took place during the process. Integrating the velocity field at the post-processing step is recommended to monitor the material's mobility. To track the particles, the ODE must be solved using an appropriate temporal integration strategy. The material points must also be located using a search approach if Eulerian or ALE meshes are being used. Alfaro et al. [165] addressed the issue of quantitatively modelling the process as well. The FSW has special traits, such as the spinning pin's high speed and exceptionally large deformations, which pose difficulties for FE methods. Meshless approaches considerably reduce these problems, allowing the simulation to use an updated Lagrangian framework.

6.6 Computational time and cost

Computational time reveals the model's efficiency, which has a substantial influence on the cost, based on a variety of created models and literature data from other models. Mesh distortions, wave speed, and mesh sizes all affect computing time in FSW/P modelling. Therefore, mesh distortions should be decreased to lessen computational costs. For friction stir technology, early FE packages took more than 7 days' worth of simulation runtime to mimic just a second of the real processing setup [166]. Some formulation

techniques, like as ALE, needed a record-breaking 2 weeks of real operating time to simulate the FSW process [167]. In the simulations before, the Intel Xeon "R" with fourteen cores operating at 2.6 GHz and 64 GB of RAM was used for the mass scaling CEL formulation [76]. This modelling method required an overall run time of almost 3 days to replicate 41 s of real processing time. It proves how effective the model they used in their research was at simulating FSP. The use of such techniques improves the efficiency of this model when compared to concurrent CEL models for FSW processes. The CEL formulation does not need a fine-quality mesh to solve mesh distortion in the mass scaling approach, nor does it need any re-meshing or remapping to increase computing performance. To increase modelling efficiency, subjective meshing is used to create a finer mesh in the interaction zone and a thicker or rougher mesh on the sides. The simulation run time for the friction stir process was greatly shortened thanks to recent developments in finite element packages and computational tools [126]. Fraser's research in science led to the creation of the ground-breaking numerical simulation programme SPHriction-3D, which was used to identify the ideal FSW process parameters. All process phases may be replicated using a phenomenological method since this special numerical technique is meshless. Their results were of the highest engineering calibre and were acquired quickly, cutting down the time from months to weeks to hours. Because the mesh-free code was created to run in parallel on the GPU, this is possible. This led to the development of a unique simulation method for the entire FSW/P that is useful for use with mono and hybrid composites. The SPH approach might provide a comprehensive understanding of the material flow, stirring, and mixing of various material combinations. One may experiment with changing a number of process parameters to further optimise the physical trials since such an advanced pattern of SPH with GPU requires less calculation time.

7 Summary

Despite the fact that the FSP has applications in many important disciplines, numerical studies are still in their infancy. In implementing the numerical approach, experimental trials, which involve high costs, resources in determining the material properties, and defining process-specific parameters for obtaining optimized output at unusual aspects of the process, can be minimized. The numerical study of FSP is still fraught with difficulties. It was evident that a thorough characterization of FSP behaviour is unattainable since FSP is a complicated phenomenon involving several interconnected mechanisms and thermal processes. Because the behaviour of the processed material is impacted by a variety of parameters in combination, precise and reliable numerical analysis of the FSP remains a challenging operation. Though different numerical methods and modelling strategies have been examined in recent years, several significant concerns and challenges in numerical modelling are addressed in various aspects of formulation strategies, process parameters and their effects, temperature distribution, capabilities of several FEA software, and the advancement towards the numerical study of friction stir processed composites. Later, material flow modelling followed by the thermal analysis was addressed to understand the thermomechanical behavior of FSP, as for every recent application, it has largely remained consistent. Nevertheless, it is tough and tricky to capture the material flow and thermal distribution at the micro-level and will not handle the large deformations of the materials, which is the most common occurrence in FSP. FSP without any reinforcement material itself is a complex process involving a blend of physical and thermal techniques. Therefore, advanced simulation tools are needed to analyze the material transfer, reinforcement distribution, and thermal distributions.

Numerous physical studies on mono and hybrid composites are carried out, whereas few numerical models account for the thermo-mechanical conditions that emerge throughout the FSP process, especially in surface composites. The main primary difficulty in modelling the composites is the compatibility of the FEM package, high-performance computing (HPC), and extreme mesh distortions leading to solver termination. Thus, the appropriate selection of formulation technique viz. Lagrangian, Eulerian, ALE, Apropos, CEL or SPH approach is needed. As a result, all these things in a single simulation tool would be able to develop a numerical model of mono and hybrid surface composites in FSP, which is still in progress. It remains one of the major goals that many researchers are interested in pursuing.

In addition, the simulation of various reinforcement combinations with varied characteristics might spark interest in the society of research. Investigators have yet to thoroughly comprehend the numerical modelling of high processing speed since it enhances the problem of divergence. Further, it would affect the simulation time and lead to the failure of the model. TTA, PD and axial force are the key factors in determining the defect-free and uniformity of the process. However, observations of their influence on heat generation and particle movement are still scarce. Additionally, one of the essential parameters in the simulation of FSP is the contact viz. COF value. An appropriate computation of the surface contact involving temperature-dependent COF values has not been wholly realized. Moreover, past studies have observed that the effect of change in tool direction after each pass is not fully addressed with its correlation to temperature distribution and material flow. It can be evident that most studies concentrate on temperature distribution and heat generation of homogeneous materials. There is a

paucity of understanding about the simulation of the particle distribution. Lastly, the review provides a practical guide for researchers and practitioners working on FSW/FSP, helping them to design optimized processes for various materials. Overall, the review serves as a valuable resource for readers looking to gain a deeper understanding of the numerical modelling techniques in FSW/P and their applications.

Supplementary Information The online version contains supplementary material available at https://doi.org/10.1007/s43452-023-00688-6.

Funding No funding was received.

Data availability Not Applicable.

Declarations

Conflict of interest The authors declare no competing interests.

Ethical approval This article does not contain any studies with human participants performed by any of the authors.

Informed consent Not applicable.

References

1. Thomas WM, Nicholas ED, Needham JC, Murch MG, Temple-Smith P, Dawes CJ. "Friction-Stir Butt Welding", GB Patent No. 9125978.8, International patent application No. PCT/GB92/02203, 1991
2. Mishra RS, Mahoney MW, McFadden SX, Mara NA, Mukherjee AK. High strain rate superplasticity in a friction stir processed 7075 Al alloy. Scr Mater. 1999;42(2):163–8. https://doi.org/10.1016/S1359-6462(99)00329-2.
3. Mishra RS, De PS, Kumar N. Friction stir welding and processing. Sci Eng. 2014. https://doi.org/10.1007/978-3-319-07043-8.
4. Mishra RS, Ma ZY, Charit I. Friction stir processing: a novel technique for fabrication of surface composite. Mater Sci Eng A. 2003;341(1–2):307–10. https://doi.org/10.1016/S0921-5093(02)00199-5.
5. Ma ZY. Friction stir processing technology: a review. Metall Mater Trans A Phys Metall Mater Sci. 2008;39A(3):642–58. https://doi.org/10.1007/s11661-007-9459-0.
6. Srivastava AK, et al. 20th century uninterrupted growth in friction stir processing of lightweight composites and alloys. Mater Chem Phys. 2021. https://doi.org/10.1016/j.matchemphys.2021.124572.
7. Zykova AP, Tarasov SY, Chumaevskiy AV, Kolubaev EA. A review of friction stir processing of structural metallic materials: process, properties, and methods. Metals (Basel). 2020;10(6):1–35. https://doi.org/10.3390/met10060772.
8. Gerlich AP. Critical assessment: friction stir processing, potential, and problems. Mater Sci Technol (United Kingdom). 2017;33(10):1139–44. https://doi.org/10.1080/02670836.2017.1300420.
9. Kumar S. Ultrasonic assisted friction stir processing of 6063 aluminum alloy. Arch Civ Mech Eng. 2016;16(3):473–84. https://doi.org/10.1016/j.acme.2016.03.002.
10. Bahrami A, Pech-Canul MI, Soltani N, Gutiérrez CA, Kamm PH, Gurlo A. Tailoring microstructure and properties of bilayer-graded Al/B4C/$MgAl_2O_4$ composites by single-stage pressureless infiltration. J Alloys Compd. 2017;694:408–18. https://doi.org/10.1016/j.jallcom.2016.09.284.
11. Węglowski MS. Friction stir processing—state of the art. Arch Civ Mech Eng. 2018;18(1):114–29. https://doi.org/10.1016/j.acme.2017.06.002.
12. Ma ZY, Mishra RS, Mahoney MW. Superplasticity in cast A356 induced via friction stir processing. Scr Mater. 2004;50(7):931–5. https://doi.org/10.1016/j.scriptamat.2004.01.012.
13. Li K, Liu X, Zhao Y. Research status and prospect of friction stir processing technology. Coatings. 2019. https://doi.org/10.3390/COATINGS9020129.
14. Srinivasan C, Karunanithi M. Fabrication of surface level Cu/SiCp nanocomposites by friction stir processing route. J Nanotechnol. 2015. https://doi.org/10.1155/2015/612617.
15. Kurt A, Uygur I, Cete E. Surface modification of aluminium by friction stir processing. J Mater Process Technol. 2011;211(3):313–7. https://doi.org/10.1016/j.jmatprotec.2010.09.020.
16. Gangil N, Siddiquee AN, Maheshwari S. Aluminium based in-situ composite fabrication through friction stir processing: a review. J Alloys Compd. 2017;715:91–104. https://doi.org/10.1016/j.jallcom.2017.04.309.
17. Sunil BR, Reddy GPK, Patle H, Dumpala R. Magnesium based surface metal matrix composites by friction stir processing. J Magnes Alloy. 2016;4(1):52–61. https://doi.org/10.1016/j.jma.2016.02.001.
18. Harwani D, Badheka V, Patel V, Li W, Andersson J. Developing superplasticity in magnesium alloys with the help of friction stir processing and its variants—a review. J Mater Res Technol. 2021;12(April):2055–75. https://doi.org/10.1016/j.jmrt.2021.03.115.
19. Wang W, et al. Friction stir processing of magnesium alloys: a review. Acta Metall Sin English Lett. 2020;33(1):43–57. https://doi.org/10.1007/s40195-019-00971-7.
20. Singh VP, Patel SK, Ranjan A, Kuriachen B. Recent research progress in solid state friction-stir welding of aluminium–magnesium alloys: a critical review. J Mater Res Technol. 2020;9(3):6217–56. https://doi.org/10.1016/j.jmrt.2020.01.008.
21. Mishra RS, Ma ZY. Friction stir welding and processing. Mater Sci Eng R Rep. 2005;50(1–2):1–78. https://doi.org/10.1016/j.mser.2005.07.001.
22. Patil NA, Pedapati SR, Mamat OB. A review on aluminium hybrid surface composite fabrication using friction stir processing. Arch Metall Mater. 2020;65(1):441–57. https://doi.org/10.24425/amm.2020.131747.
23. Bharti S, Hetiya ND, Patel KM. A review on manufacturing the surface composites by friction stir processing. Mater Manuf Process. 2021;36(2):135–70. https://doi.org/10.1080/10426914.2020.1813897.
24. Sharma DK, Badheka V, Patel V, Upadhyay G. Recent developments in hybrid surface metal matrix composites produced by friction stir processing: a review. J Tribol. 2021. https://doi.org/10.1115/1.4049590.
25. He X, Gu F, Ball A. A review of numerical analysis of friction stir welding. Prog Mater Sci. 2014;65:1–66. https://doi.org/10.1016/j.pmatsci.2014.03.003.
26. Bahari MS, Jaffarullah MS, Mohamed Z. Heat analysis in friction stir welding using finite element method. J Mech Eng. 2018;5(Specialissue4):174–88.
27. Schmidt HNB, Dickerson TL, Hattel JH. Material flow in butt friction stir welds in AA2024-T3. Acta Mater. 2006;54(4):1199–209. https://doi.org/10.1016/j.actamat.2005.10.052.
28. Nandan R, Roy GG, Lienert TJ, Debroy T. Numerical modelling of 3D plastic flow and heat transfer during friction stir welding of stainless steel. Sci Technol Weld Join. 2006;11(5):526–37. https://doi.org/10.1179/174329306X107692.

29. Derazkola HA, Garcia E, Elyasi M. Underwater friction stir welding of PC: Experimental study and thermo-mechanical modelling. J Manuf Process. 2021;65(January):161–73. https://doi.org/10.1016/j.jmapro.2021.03.034.
30. Wan ZY, Zhang Z, Zhou X. Finite element modeling of grain growth by point tracking method in friction stir welding of AA6082-T6. Int J Adv Manuf Technol. 2017;90(9–12):3567–74. https://doi.org/10.1007/s00170-016-9632-y.
31. Fashami HAA, Arab NBM, Gollo MH, Nami B. Numerical and experimental investigation of defects formation during friction stir processing on AZ91. SN Appl Sci. 2021. https://doi.org/10.1007/s42452-020-04032-y.
32. Mehdi H, Mishra RS. Effect of friction stir processing on mechanical properties and heat transfer of TIG welded joint of AA6061 and AA7075. Def Technol. 2020. https://doi.org/10.1016/j.dt.2020.04.014.
33. Cremonesi M, Meduri S, Perego U, Frangi A. An explicit Lagrangian finite element method for free-surface weakly compressible flows. Comput Part Mech. 2017;4(3):357–69. https://doi.org/10.1007/s40571-016-0122-7.
34. Jain R, Pal SK, Singh SB. Numerical modeling methodologies for friction stir welding process. Elsevier Ltd. 2017. https://doi.org/10.1016/B978-0-85709-481-0.00005-7.
35. Ritti L, Bhat T. Design and numerical analysis of tool for FSP simulation of magnesium alloys. Mater Today Proc. 2021;46:2489–97. https://doi.org/10.1016/j.matpr.2021.01.414.
36. Buffa G, Fratini L. Friction stir welding of steels: Process design through continuum based FEM model. Sci Technol Weld Join. 2009;14(3):239–46. https://doi.org/10.1179/136217109X421328.
37. Buffa G, Hua J, Shivpuri R, Fratini L. A continuum based fem model for friction stir welding—model development. Mater Sci Eng A. 2006;419(1–2):389–96. https://doi.org/10.1016/j.msea.2005.09.040.
38. Nielsen KL. Ductile damage development in friction stir welded aluminum (AA2024) joints. Eng Fract Mech. 2008;75(10):2795–811. https://doi.org/10.1016/j.engfracmech.2008.01.012.
39. Vignesh RV, Padmanaban R. Modelling of peak temperature during friction stir processing of magnesium alloy AZ91. IOP Conf Ser Mater Sci Eng. 2018. https://doi.org/10.1088/1757-899X/310/1/012019.
40. Asadi P, Givi MKB, Akbari M. Microstructural simulation of friction stir welding using a cellular automaton method: a microstructure prediction of AZ91 magnesium alloy. Int J Mech Mater Eng. 2015. https://doi.org/10.1186/s40712-015-0048-5.
41. Asadi P, Givi MKB, Akbari M. Simulation of dynamic recrystallization process during friction stir welding of AZ91 magnesium alloy. Int J Adv Manuf Technol. 2016;83(1–4):301–11. https://doi.org/10.1007/s00170-015-7595-z.
42. Boscheri W, Dumbser M. High order accurate direct Arbitrary-Lagrangian–Eulerian ADER-WENO finite volume schemes on moving curvilinear unstructured meshes. Comput Fluids. 2016;136:48–66. https://doi.org/10.1016/j.compfluid.2016.05.020.
43. Priyadarshini A, Pal SK, Samantaray AK. Finite element modeling of chip formation in orthogonal machining. Stat Comput Tech Manuf. 2012;9783642258:101–44. https://doi.org/10.1007/978-3-642-25859-6_3.
44. Bastier A, Maitournam MH, Roger F, Van KD. Modelling of the residual state of friction stir welded plates. J Mater Process Technol. 2008;200(1–3):25–37. https://doi.org/10.1016/j.jmatprotec.2007.10.083.
45. Braeunig J-P, Chaudet B. Study of a collocated Lagrange-remap scheme for multi-material flows adapted to HPC. Int J Numer Methods Fluids. 2016. https://doi.org/10.1002/fld.428.
46. Cho JH, Dawson PR. Investigation on texture evolution during friction stir welding of stainless steel. Metall Mater Trans A Phys Metall Mater Sci. 2006;37(4):1147–64. https://doi.org/10.1007/s11661-006-1093-8.
47. Cho JH, Boyce DE, Dawson PR. Modelling of strain hardening during friction stir welding of stainless steel. Model Simul Mater Sci Eng. 2007;15(5):469–86. https://doi.org/10.1088/0965-0393/15/5/007.
48. Cho JH, Boyce DE, Dawson PR. Modeling strain hardening and texture evolution in friction stir welding of stainless steel. Mater Sci Eng A. 2005;398(1–2):146–63. https://doi.org/10.1016/j.msea.2005.03.002.
49. Feulvarch E, Roux JC, Bergheau JM. A simple and robust moving mesh technique for the finite element simulation of friction stir welding. J Comput Appl Math. 2013;246:269–77. https://doi.org/10.1016/j.cam.2012.07.013.
50. Meyghani B, Awang M. The influence of the tool tilt angle on the heat generation and the material behavior in friction stir welding (FSW). Metals (Basel). 2022. https://doi.org/10.21203/rs.3.rs-1984818/v1License.
51. Meyghani B, Awang MB, Emamian SS, Nor MKBM, Pedapati SR. A comparison of different finite element methods in the thermal analysis of friction stir welding (FSW). Metals (Basel). 2017;7(10):1–23. https://doi.org/10.3390/met7100450.
52. Altair University, Introduction to Explicit Analysis with Radioss. 2020.
53. Zhang Z, Liu YL, Chen JT. Effect of shoulder size on the temperature rise and the material deformation in friction stir welding. Int J Adv Manuf Technol. 2009;45(9–10):889–95. https://doi.org/10.1007/s00170-009-2034-7.
54. Fratini L, Buffa G. Continuous dynamic recrystallization phenomena modelling in friction stir welding of aluminium alloys: a neural-network-based approach. Proc Inst Mech Eng Part B J Eng Manuf. 2007;221(5):857–64. https://doi.org/10.1243/09544054JEM674.
55. Bagheri B, Abdollahzadeh A, Abbasi M, Kokabi AH. Effect of vibration on machining and mechanical properties of AZ91 alloy during FSP: modeling and experiments. Int J Mater Form. 2020. https://doi.org/10.1007/s12289-020-01551-2.
56. Chen C, Kovacevic R. Thermomechanical modelling and force analysis of friction stir welding by the finite element method. Proc Inst Mech Eng Part C J Mech Eng Sci. 2004;218(5):509–20. https://doi.org/10.1243/095440604323052292.
57. Chenot JL, Massoni E. Finite element modelling and control of new metal forming processes. Int J Mach Tools Manuf. 2006;46(11):1194–200. https://doi.org/10.1016/j.ijmachtools.2006.01.031.
58. Buffa G, Hua J, Shivpuri R, Fratini L. Design of the friction stir welding tool using the continuum based FEM model. Mater Sci Eng A. 2006;419(1–2):381–8. https://doi.org/10.1016/j.msea.2005.09.041.
59. Khandkar MZH, Khan JA, Reynolds AP, Sutton MA. Predicting residual thermal stresses in friction stir welded metals. J Mater Process Technol. 2006;174(1–3):195–203. https://doi.org/10.1016/j.jmatprotec.2005.12.013.
60. Jain R, Pal SK, Singh SB. Thermomechanical simulation of friction stir welding process using Lagrangian method; 2018, p. 103–146. https://doi.org/10.1007/978-981-10-8518-5_4.
61. Gök K, Aydin M. Investigations of friction stir welding process using finite element method. Int J Adv Manuf Technol. 2013;68(1–4):775–80. https://doi.org/10.1007/s00170-013-4798-z.
62. Colegrove PA, Shercliff HR. Development of Trivex friction stir welding tool part 1—two-dimensional flow modelling and experimental validation. Sci Technol Weld Join. 2004;9(4):345–51. https://doi.org/10.1179/136217104225021670.

63. Colegrove PA, Shercliff HR. Development of Trivex friction stir welding tool Part 2—three-dimensional flow modelling. Sci Technol Weld Join. 2004;9(4):352–61. https://doi.org/10.1179/136217104225021661.
64. Contuzzi N, Campanelli SL, Casalino G, Ludovico AD. On the role of the thermal contact conductance during the friction stir welding of an AA5754-H111 butt joint. Appl Therm Eng. 2016;104:263–73. https://doi.org/10.1016/j.applthermaleng.2016.05.071.
65. Miles MP, Nelson TW, Gunter C, Liu FC, Fourment L, Mathis T. Predicting recrystallized grain size in friction stir processed 304L stainless steel. J Mater Sci Technol. 2019;35(4):491–8. https://doi.org/10.1016/j.jmst.2018.10.021.
66. Ren JG, Wang L, Xu DK, Xie LY, Zhang ZC. Analysis and modeling of friction stir processing-based crack repairing in 2024 aluminum alloy. Acta Metall Sin English Lett. 2017;30(3):228–37. https://doi.org/10.1007/s40195-016-0489-8.
67. Bellala SSK, Pedapati SR, Marode RV (2022) Comparative study of thermal modelling using Eulerian and SPH techniques for FSW. In: IET digital library, engineering technology international conference (ETIC 2022); 2022. p. 76–82. https://doi.org/10.1049/ICP.2022.2573.
68. Hamilton R, Mackenzie D, Li H. Multi-physics simulation of friction stir welding process. Eng Comput (Swansea, Wales). 2010;27(8):967–85. https://doi.org/10.1108/02644401011082980.
69. Chiumenti M, Cervera M, Agelet de Saracibar C, Dialami N. Numerical modeling of friction stir welding processes. Comput Methods Appl Mech Eng. 2013;254:353–69. https://doi.org/10.1016/j.cma.2012.09.013.
70. Yu Z, Zhang W, Choo H, Feng Z. Transient heat and material flow modeling of friction stir processing of magnesium alloy using threaded tool. Metall Mater Trans A Phys Metall Mater Sci. 2012;43(2):724–37. https://doi.org/10.1007/s11661-011-0862-1.
71. Fashami HAA, Arab NBM, Gollo MH, Nami B. Effect of multi-pass friction stir processing on thermal distribution and mechanical properties of AZ91. Mech Ind. 2020. https://doi.org/10.1051/meca/2020042.
72. Agha H, Fashami A, Hoseinpour M. The numerical modeling to study the multi-pass friction stir processing on magnesium casting alloy AZ91. Int J Adv Des Manuf Technol. 2019;12(4):9–16.
73. Mimouni O, Badji R, Hadji M, Kouadri-David A, Rachid H, Chekroun N. Numerical simulation of temperature distribution and material flow during friction stir welding 2017A aluminum alloys. MS T 2019 Mater Sci Technol. 2019;12002:1034–40. https://doi.org/10.7449/2019/MST_2019_1034_1040.
74. Benson DJ. A mixture theory for contact in multi-material Eulerian formulations. Comput Methods Appl Mech Eng. 1997;140(1–2):59–86. https://doi.org/10.1016/S0045-7825(96)01050-X.
75. Adetunla A, Akinlabi, E. Finite element analysis of the heat generated during FSP of 1100 Al alloy. 2019. https://doi.org/10.1007/978-981-15-5753-8_37.
76. Ansari MA, Samanta A, Behnagh RA, Ding H. An efficient coupled Eulerian–Lagrangian finite element model for friction stir processing. Int J Adv Manuf Technol. 2019;101(5–8):1495–508. https://doi.org/10.1007/s00170-018-3000-z.
77. Dialami N, Chiumenti M, Cervera M, Agelet De Saracibar C. An apropos kinematic framework for the numerical modeling of friction stir welding. Comput Struct. 2013;117:48–57. https://doi.org/10.1016/j.compstruc.2012.12.006.
78. Dialami N, Cervera M, Chiumenti M, de Saracibar CA. A fast and accurate two-stage strategy to evaluate the effect of the pin tool profile on metal flow, torque and forces in friction stir welding. Int J Mech Sci. 2017;122(November):215–27. https://doi.org/10.1016/j.ijmecsci.2016.12.016.
79. Gingold RA, Monaghan JJ. Smoothed particle hydrodynamics: theory and application to non-spherical stars. Mon Not R Astron Soc. 1977;181(3):375–89. https://doi.org/10.1093/MNRAS/181.3.375.
80. Monaghan JJ. Smoothed particle hydrodynamics. Annu Rev Astron Astrophys. 1992;30(1):543–74. https://doi.org/10.1146/annurev.aa.30.090192.002551.
81. Monaghan JJ. Smoothed particle hydrodynamics. Rep Prog Phys. 2005;68(8):1703. https://doi.org/10.1088/0034-4885/68/8/R01.
82. Tartakovsky AM, Ferris KF, Meakin P. Lagrangian particle model for multiphase flows. Comput Phys Commun. 2009;180(10):1874–81. https://doi.org/10.1016/j.cpc.2009.06.002.
83. Monaghan JJ, Kajtar JB. SPH particle boundary forces for arbitrary boundaries. Comput Phys Commun. 2009;180(10):1811–20. https://doi.org/10.1016/J.CPC.2009.05.008.
84. Benz W, Asphaug E. Simulations of brittle solids using SPH. Comput Phys Commun. 1995;87:253–65.
85. Cleary PW, Ha J. Three dimensional modelling of high pressure die casting. Int J Cast Met Res. 2000;12(6):357–65. https://doi.org/10.1080/13640461.2000.11819373.
86. Pan W, Li D, Tartakovsky AM, Ahzi S, Khraisheh M, Khaleel M. A new smoothed particle hydrodynamics non-Newtonian model for friction stir welding: Process modeling and simulation of microstructure evolution in a magnesium alloy. Int J Plast. 2013;48:189–204. https://doi.org/10.1016/j.ijplas.2013.02.013.
87. Fraser KA, St-Georges L, Kiss LI. Prediction of defects in a friction stir welded joint using the smoothed particle hydrodynamics method. 2013. https://www.researchgate.net/publication/275271401. Accessed 20 Apr 2023.
88. Fraser K, Kiss LI, St-Georges L, Drolet D. "Optimization of friction stir weld joint quality using a meshfree fully-coupled thermo-mechanics approach. Metals (Basel). 2018. https://doi.org/10.3390/met8020101.
89. Ansari MA, Behnagh RA. Numerical study of friction stir welding (FSW) plunging phase using smoothed particle hydrodynamics (SPH). Model Simul Mater Sci Eng. 2019. https://doi.org/10.1088/1361-651X/ab1ca7.
90. Meyghani B, Awang MB, Wu CS. Thermal analysis of friction stir processing (FSP) using arbitrary Lagrangian–Eulerian (ALE) and smoothed particle hydrodynamics (SPH) meshing techniques. Materwiss Werksttech. 2020;51(5):550–7. https://doi.org/10.1002/mawe.201900222.
91. Meyghani B, Awang M, Wu CS, Emamian S. Temperature distribution investigation during friction stir welding (FSW) using smoothed-particle hydrodynamics (SPH). Lect Notes Mech Eng. 2020. https://doi.org/10.1007/978-981-15-5753-8_70.
92. Vacondio R, et al. Grand challenges for smoothed particle hydrodynamics numerical schemes. Comput Part Mech. 2021;8(3):575–88. https://doi.org/10.1007/s40571-020-00354-1.
93. Ebrahimzad P, Ghasempar M, Balali M. Friction stir processing of aerospace aluminum alloy by addition of carbon nano tube. Trans Indian Inst Met. 2017;70(9):2241–53. https://doi.org/10.1007/s12666-017-1062-5.
94. Marode RV, Pedapati SR, Lemma TA. Effect of process parameters on AZ91/SiC surface composites for lightweight E-vehicles. In 2022 7th international conference on electric vehicular technology (ICEVT); 2022. p. 109–115. https://doi.org/10.1109/ICEVT55516.2022.9924699.
95. Farghadani M, Karimzadeh F, Enayati MH, Naghshehkesh N, Moghaddam AO. Fabrication of AZ91D/Cu/Mg_2Cu and AZ91D/Mg_2Cu/$MgCu_2$/MgO in-situ hybrid surface nanocomposites via friction stir processing. Surf Topogr Metrol Prop. 2020. https://doi.org/10.1088/2051-672X/abb527.
96. Yousefpour F, Jamaati R, Aval HJ. Synergistic effects of hybrid (HA+Ag) particles and friction stir processing in the design of

a high-strength magnesium matrix bio-nano composite with an appropriate texture for biomedical applications. J Mech Behav Biomed Mater. 2022;125:104983. https://doi.org/10.1016/j.jmbbm.2021.104983.
97. Tutunchilar S, Haghpanahi M, Givi MKB, Asadi P, Bahemmat P. Simulation of material flow in friction stir processing of a cast Al–Si alloy. Mater Des. 2012;40:415–26. https://doi.org/10.1016/j.matdes.2012.04.001.
98. Bussetta P, et al. Comparison of a fluid and a solid approach for the numerical simulation of friction stir welding with a non-cylindrical pin. Steel Res Int. 2014;85(6):968–79. https://doi.org/10.1002/srin.201300182.
99. Dialami N, Chiumenti M, Cervera M, Agelet de Saracibar C, Ponthot JP. Material flow visualization in friction stir welding via particle tracing. Int J Mater Form. 2015;8(2):167–81. https://doi.org/10.1007/s12289-013-1157-4.
100. Salloomi KN. Fully coupled thermomechanical simulation of friction stir welding of aluminum 6061–T6 alloy T-joint. J Manuf Process. 2019;45:746–54. https://doi.org/10.1016/j.jmapro.2019.06.030.
101. Saha R, Biswas P. Temperature and stress evaluation during friction stir welding of inconel 718 alloy using finite element numerical simulation. J Mater Eng Perform. 2021;31(3):2002–11. https://doi.org/10.1007/s11665-021-06313-y.
102. Wang C, Deng J, Dong C, Zhao Y. Numerical simulation and experimental studies on stationary shoulder friction stir welding of aluminum alloy T-Joint. Front Mater. 2022;9:898929. https://doi.org/10.3389/fmats.2022.898929.
103. Mishin V, et al. Numerical simulation of the thermo-mechanical behavior of 6061 aluminum alloy during friction-stir welding. J Manuf Mater Process. 2022;6(4):68. https://doi.org/10.3390/jmmp6040068.
104. Zhu Z, Wang M, Zhang H, Zhang X, Yu T, Wu Z. A finite element model to simulate defect formation during friction stir welding. Metals (Basel). 2017. https://doi.org/10.3390/met7070256.
105. Shamanian M, Mostaan H, Safari M, Dezfooli MS. Friction-stir processing of Al-12%Si alloys: grain refinement, numerical simulation, microstructure evolution, dry sliding wear performance and hardness measurement. Metall Res Technol. 2017. https://doi.org/10.1051/metal/2016066.
106. Salih OS, Ou H, Sun W. Heat generation, plastic deformation and residual stresses in friction stir welding of aluminium alloy. Int J Mech Sci. 2022. https://doi.org/10.1016/j.ijmecsci.2022.107827.
107. Bhojwani S. Smoothed particle hydrodynamics modeling of the friction stir welding process. The University of Texas At El Paso; 2007.
108. Timesli A, Zahrouni H, Braikat B, Moufki A, Lahmam H. Numerical Model Based on Meshless Method to Simulate FSW. In Proceedings of the Particle-Based Methods II - Fundamentals and Applications. 2011;651–662
109. Yang HG. Numerical simulation of the temperature and stress state on the additive friction stir with the smoothed particle hydrodynamics method. Strength Mater. 2020;52(1):24–31. https://doi.org/10.1007/s11223-020-00146-1.
110. Eivani AR, Vafaeenezhad H, Jafarian HR, Zhou J. A novel approach to determine residual stress field during FSW of AZ91 Mg alloy using combined smoothed particle hydrodynamics/neuro-fuzzy computations and ultrasonic testing. J Magnes Alloy. 2021;9(4):1304–28. https://doi.org/10.1016/j.jma.2020.11.018.
111. Shishova E, Panzer F, Werz M, Eberhard P. Reversible interparticle bonding in SPH for improved simulation of friction stir welding. Comput Part Mech. 2022. https://doi.org/10.1007/s40571-022-00510-9.
112. Marode RV, Pedapati SR, Lemma TA, Somi V, Janga R. Thermo-mechanical modelling of friction stir processing of AZ91 alloy: using smoothed-particle hydrodynamics. Lubricants. 2022;10(12):1–20. https://doi.org/10.3390/lubricants10120355.
113. Zinati RF, Razfar MR. Finite element simulation and experimental investigation of friction stir processing of Polyamide 6. Proc Inst Mech Eng Part B J Eng Manuf. 2015;229(12):2205–15. https://doi.org/10.1177/0954405414546705.
114. Shojaeefard MH, Akbari M, Khalkhali A, Asadi P. Effect of tool pin profile on distribution of reinforcement particles during friction stir processing of B4C/aluminum composites. Proc Inst Mech Eng Part L J Mater Des Appl. 2018;232(8):637–51. https://doi.org/10.1177/1464420716642471.
115. Shojaeefard MH, Akbari M, Asadi P, Khalkhali A. The effect of reinforcement type on the microstructure, mechanical properties, and wear resistance of A356 matrix composites produced by FSP. Int J Adv Manuf Technol. 2017;91(1–4):1391–407. https://doi.org/10.1007/s00170-016-9853-0.
116. Asadi P, Givi MKB, Rastgoo A, Akbari M, Zakeri V, Rasouli S. Predicting the grain size and hardness of AZ91/SiC nanocomposite by artificial neural networks. Int J Adv Manuf Technol. 2012;63(9–12):1095–107. https://doi.org/10.1007/s00170-012-3972-z.
117. Santos TG, Lopes N, MacHado M, Vilaça P, Miranda RM. Surface reinforcement of AA5083-H111 by friction stir processing assisted by electrical current. J Mater Process Technol. 2015;216:375–80. https://doi.org/10.1016/j.jmatprotec.2014.10.005.
118. Aziz SB, Dewan MW, Huggett DJ, Wahab MA, Okeil AM, Liao TW. Impact of Friction Stir Welding (FSW) process parameters on thermal modeling and heat generation of aluminum alloy joints. Acta Metall Sin English Lett. 2016;29(9):869–83. https://doi.org/10.1007/s40195-016-0466-2.
119. Al-Badour F, Merah N, Shuaib A, Bazoune A. Coupled Eulerian Lagrangian finite element modeling of friction stir welding processes. J Mater Process Technol. 2013;213(8):1433–9. https://doi.org/10.1016/j.jmatprotec.2013.02.014.
120. Nandan R, DebRoy T, Bhadeshia HKDH. Recent advances in friction-stir welding—process, weldment structure and properties. Prog Mater Sci. 2008;53(6):980–1023. https://doi.org/10.1016/j.pmatsci.2008.05.001.
121. Ammouri AH, Kheireddine AH, Kridli GT, Hamade RF. FEM optimization of process parameters and in-process cooling in the friction stir processing of magnesium alloy AZ31B. ASME Int Mech Eng Congr Expo Proc. 2013. https://doi.org/10.1115/IMECE2013-62468.
122. Janga VSR, Awang M, Yamin MF, Suhuddin UFH, Klusemann B, Dos Santos JF. Experimental and numerical analysis of refill friction stir spot welding of thin AA7075-T6 sheets. Materials (Basel). 2021;14(23):1–21. https://doi.org/10.3390/ma14237485.
123. Kuykendall K, Nelson T, Sorensen C. On the selection of constitutive laws used in modeling friction stir welding. Int J Mach Tools Manuf. 2013;74:74–85. https://doi.org/10.1016/j.ijmachtools.2013.07.004.
124. Meyghani B, Awang M, Emamian S. A comparative study of finite element analysis for friction stir welding application. ARPN J Eng Appl Sci. 2016;11(22):12984–9.
125. Kang SW, Jang BS. A study on computational fluid dynamics simulation of friction stir welding. Anal. Des. Mar. Struct.—Proceedings of 4th International Conference Marine Structure. MARSTRUCT 2013, no. October; 2013. p. 433–439. https://doi.org/10.1201/b15120-59.
126. Fraser K. Robust and efficient meshfree solid thermo-mechanics simulation of friction stir welding. 2017. https://doi.org/10.13140/RG.2.2.13318.68169.
127. Fraser KA, St-Georges L, Kiss LI, Chiricota Y. Hybrid thermo-mechanical contact algorithm for 3D SPH-FEM multi-physics simulations. Proceedings of 4th International Conference Part.

Methods—Fundam. Appl. Part. 2015, no. September; 2015. p. 275–286.
128. Pramanik A, Sanghvi H, Basak AK. Modern manufacturing engineering. 2015. https://doi.org/10.1007/978-3-319-20152-8.
129. Schmidt H, Hattel J. A local model for the thermomechanical conditions in friction stir welding. Model Simul Mater Sci Eng. 2005;13(1):77–93. https://doi.org/10.1088/0965-0393/13/1/006.
130. Kim D, et al. Numerical simulation of friction stir butt welding process for AA5083-H18 sheets. Eur J Mech A Solids. 2010;29(2):204–15. https://doi.org/10.1016/j.euromechsol.2009.10.006.
131. Patil S, Tay YY, Baratzadeh F, Lankarani H. Modeling of friction-stir butt-welds and its application in automotive bumper impact performance Part 2. Impact modeling and bumper crash performance. J Mech Sci Technol. 2017;31(7):3225–32. https://doi.org/10.1007/s12206-017-0612-4.
132. Babu N, Karunakaran N, Balasubramanian V. Numerical predictions and experimental investigation of the temperature distribution of friction stir welded AA 5059 aluminium alloy joints. Int J Mater Res. 2017;108(1):68–75. https://doi.org/10.3139/146.111448.
133. Chen G, Zhang S, Zhu Y, Yang C, Shi Q. Thermo-mechanical analysis of friction stir welding: a review on recent advances. Acta Metall Sin English Lett. 2020;33(1):3–12. https://doi.org/10.1007/s40195-019-00942-y.
134. Schmidt H, Hattel J, Wert J. An analytical model for the heat generation in friction stir welding. Model Simul Mater Sci Eng. 2004;12(1):143–57. https://doi.org/10.1088/0965-0393/12/1/013.
135. Kishta EEM, Abed FH, Darras BM. Nonlinear finite element simulation of friction stir processing of marine grade 5083 aluminum alloy. Eng Trans. 2014;62(4):313–28.
136. Asadi P, Mahdavinejad RA, Tutunchilar S. Simulation and experimental investigation of FSP of AZ91 magnesium alloy. Mater Sci Eng A. 2011;528(21):6469–77. https://doi.org/10.1016/j.msea.2011.05.035.
137. Albakri AN, Mansoor B, Nassar H, Khraisheh MK. Thermo-mechanical and metallurgical aspects in friction stir processing of AZ31 Mg alloy—a numerical and experimental investigation. J Mater Process Technol. 2013;213(2):279–90. https://doi.org/10.1016/j.jmatprotec.2012.09.015.
138. Albakri AN, Mansoor B, Nassar H, Khraisheh MK. Simulation of friction stir processing with internally cooled tool. Adv Mater Res. 2012;445:560–5. https://doi.org/10.4028/www.scientific.net/AMR.445.560.
139. Ibakri AN, Aljoaba SZ, Khraisheh MK. Modelling of friction stir processing with in process cooling using computational fluid dynamics analysis. Adv Sustain Manuf. 2011. https://doi.org/10.1007/978-3-642-20183-7.
140. Cartigueyen S, Sukesh OP, Mahadevan K. Numerical and experimental investigations of heat generation during friction stir processing of copper. Procedia Eng. 2014;97:1069–78. https://doi.org/10.1016/j.proeng.2014.12.385.
141. Dong P, Lu F, Hong JK, Cao Z. Coupled thermomechanical analysis of friction stir welding process using simplified models. Sci Technol Weld Join. 2001;6(5):281–7. https://doi.org/10.1179/136217101101538884.
142. Mehdi H, Mishra RS. Analysis of material flow and heat transfer in reverse dual rotation friction stir welding: a review. Int J Steel Struct. 2019;19(2):422–34. https://doi.org/10.1007/s13296-018-0131-x.
143. Ranjan R, et al. Classification and identification of surface defects in friction stir welding: an image processing approach. J Manuf Process. 2016;22:237–53. https://doi.org/10.1016/j.jmapro.2016.03.009.
144. Memon S, Fydrych D, Fernandez AC, Derazkola HA, Derazkola HA. Effects of fsw tool plunge depth on properties of an al-mg-si alloy t-joint: thermomechanical modeling and experimental evaluation. Materials (Basel). 2021. https://doi.org/10.3390/ma14164754.
145. Türkan M, Karakaş Ö. Numerical modeling of defect formation in friction stir welding. Mater Today Commun. 2022. https://doi.org/10.1016/j.mtcomm.2022.103539.
146. Hassanamraji N, Eivani AR, Aboutalebi MR. Finite element simulation of deformation and heat transfer during friction stir processing of as-cast AZ91 magnesium alloy. J Mater Res Technol. 2021;14:2998–3017. https://doi.org/10.1016/j.jmrt.2021.08.087.
147. Zhang Z, Zhang HW. A fully coupled thermo-mechanical model of friction stir welding. Int J Adv Manuf Technol. 2008;37(3–4):279–93. https://doi.org/10.1007/s00170-007-0971-6.
148. Nassar HW, Khraisheh MK. Simulation of material flow and heat evolution in friction stir processing incorporating melting. J Eng Mater Technol Trans ASME. 2012. https://doi.org/10.1115/1.4006918.
149. Zhai M, Wu CS, Su H. Influence of tool tilt angle on heat transfer and material flow in friction stir welding. J Manuf Process. 2020;59:98–112. https://doi.org/10.1016/j.jmapro.2020.09.038.
150. Zhang S, Shi Q, Liu Q, Xie R, Zhang G, Chen G. Effects of tool tilt angle on the in-process heat transfer and mass transfer during friction stir welding. Int J Heat Mass Transf. 2018;125:32–42. https://doi.org/10.1016/j.ijheatmasstransfer.2018.04.067.
151. Dialami N, Cervera M, Chiumenti M. Effect of the tool tilt angle on the heat generation and the material flow in friction stir welding. Metals (Basel). 2019. https://doi.org/10.3390/met9010028.
152. Dialami N, Chiumenti M, Cervera M, Agelet de Saracibar C. Challenges in thermo-mechanical analysis of friction stir welding processes. Arch Comput Methods Eng. 2016;24(1):189–225. https://doi.org/10.1007/S11831-015-9163-Y.
153. Dialami N, Cervera M, Chiumenti M, de Saracibar CA. Local–global strategy for the prediction of residual stresses in FSW processes. Int J Adv Manuf Technol. 2017;88(9–12):3099–111. https://doi.org/10.1007/s00170-016-9016-3.
154. de Saracibar CA. Challenges to be tackled in the computational modeling and numerical simulation of FSW processes. Metals. 2019. https://doi.org/10.3390/met9050573.
155. Kubit A, Trzepiecinski T. A fully coupled thermo-mechanical numerical modelling of the refill friction stir spot welding process in Alclad 7075–T6 aluminium alloy sheets. Arch Civ Mech Eng. 2020. https://doi.org/10.1007/s43452-020-00127-w.
156. de Saracibar CA, Chiumenti M, Cervera M, Dialami N, Seret A. Computational modeling and sub-grid scale stabilization of incompressibility and convection in the numerical simulation of friction stir welding processes. Arch Comput Methods Eng. 2014;21(1):3–37. https://doi.org/10.1007/s11831-014-9094-z.
157. Talebi H, Froend M, Klusemann B. Application of adaptive element-free Galerkin method to simulate friction stir welding of aluminum. Procedia Eng. 2017;207:580–5. https://doi.org/10.1016/j.proeng.2017.10.1024.
158. Tutum CC, Hattel JH. Numerical optimisation of friction stir welding: Review of future challenges. Sci Technol Weld Join. 2011;16(4):318–24. https://doi.org/10.1179/1362171811Y.0000000011.
159. Awang M. Simulation of friction stir spot welding (FSSW) process: study of Friction Phenomena. 2007.
160. Janga VSR, Awang M, Yamin MF, Suhuddin UFH, Klusemann B, Dos Santos JF. Experimental and numerical analysis of refill friction stir spot welding of thin AA7075-T6 sheets. Materials (Basel). 2021;14(23):7485. https://doi.org/10.3390/ma14237485.
161. Janga VSR, Awang M. Influence of plunge depth on temperatures and material flow behavior in refill friction stir spot welding of thin AA7075-T6 sheets: a numerical study. Metals (Basel). 2022;12(6):927. https://doi.org/10.3390/met12060927.

162. Meyghani B, Wu C. Progress in thermomechanical analysis of friction stir welding. Chin J Mech Eng English Ed. 2020. https://doi.org/10.1186/s10033-020-0434-7.
163. Zhang Z. Comparison of two contact models in the simulation of friction stir welding process. J Mater Sci. 2008;43(17):5867–77. https://doi.org/10.1007/s10853-008-2865-x.
164. Dialami N, Chiumenti M, Cervera M, Agelet De Saracibar C, Ponthot JP, Bussetta P. Numerical simulation and visualization of material flow in Friction Stir Welding via particle tracing. Comput Methods Appl Sci. 2014;33:157–69. https://doi.org/10.1007/978-3-319-06136-8_7.
165. Alfaro I, Racineux G, Poitou A, Cueto E, Chinesta F. Numerical simulation of friction stir welding by natural element methods. Int J Mater Form. 2009;2(4):225–34. https://doi.org/10.1007/s12289-009-0406-z.
166. Lasley MJ. A finite element simulation of temperature and material flow in friction stir welding. 2005.
167. Assidi M, Fourment L, Guerdoux S, Nelson T. Friction model for friction stir welding process simulation: calibrations from welding experiments. Int J Mach Tools Manuf. 2010;50(2):143–55. https://doi.org/10.1016/j.ijmachtools.2009.11.008.